Structural Basis for the Reaction of Tropinone Reductase-II Analyzed by X-ray Crystallography

Atsuko Yamashita

1998

Contents

Abbreviations

ADP	adenosine 5'-diphosphate
DEAE	diethylaminoethyl
DTT	dithiothreitol
EDTA	ethylenediamine-*N*,*N*,*N'*,*N'*-tetraacetic acid
ESRF	European Synchrotron Radiation Facility
F_C	calculated structure factor
F_O	observed structure factor
FDH	formate dehydrogenase
GDH	glycerate dehydrogenase
HEPES	2-[4-(hydroxyethyl)-1-piperazinyl]ethanesulfonic acid
LDH	lactate dehydrogenase
MDR	medium-chain dehydrogenase/reductase
MES	2-morpholinoethanesulfonic acid
MIR	multiple isomorphous replacement
MIRAS	multiple isomorphous replacement method with anomalous scattering
MPD	2-methyl-2,4-pentanediol
MR	molecular replacement
NADPH	β-nicotinamide adenine dinucleotide phosphate (reduced form)
$NADP^+$	β-nicotinamide adenine dinucleotide phosphate (oxidized form)
PAGE	polyacrylamide gel electrophoresis
PEG	polyethylene glycol
r.m.s.d.	root mean square deviation
rpm	revolutions per minute
SDR	short-chain dehydrogenase/reductase
SDS	sodium dodecylsulfate
TR	tropinone reductase
Tris	tris(hydroxymethyl)aminoethane
ψ-tropine	pseudotropine
7α-HSDH	7α-hydroxysteroid dehydrogenase

CHAPTER 1

General Introduction

Tropane alkaloids are heterocyclic amine derivatives known as secondary metabolites in plants. They are produced mainly in several solanaceous species and have been utilized as pharmaceuticals because of their mydriatic and anesthetic properties. In the tropane alkaloid biosynthesis, tropinone reductase-I (TR-I, EC 1.1.1.206) and tropinone reductase-II (TR-II, EC 1.1.1.236) constitute a branching point of the metabolic pathway. TR-I catalyzes NADPH-dependent reduction of the 3-carbonyl group of tropinone to an α-hydroxyl group and produces tropine (Figure 1-1). On the other hand, TR-II reduces the same substrate tropinone using NADPH but produces pseudotropine (ψ-tropine) with a β-hydroxyl group, which has a different diastereomeric configuration from that of the product of TR-I (Figure 1-1).

The two TRs show similar kinetic behavior for NADPH, but the different behavior for the substrates. They have been purified to near homogeneity from *Hyoscyamus niger* for the first time, and characterized by Hashimoto *et al.* (Hashimoto *et al*., 1992). Both TRs have similar affinities for NADPH, and are classified as B-specific oxidoreductases, which transfer the *pro-S* hydrogen at C4 of NADPH to tropinone. On the other hand, the two TRs have different affinities for tropinone (TR-II has higher affinity than TR-I), and show different activities and inhibition patterns for substrate analogues (Hashimoto *et al*., 1992; Nakajima *et al*., 1994; Portsteffen *et al*., 1994).

The amino acid sequences of the TRs from *Datura stramonium* have been deduced from their cDNAs. The respective subunits of TR-I and TR-II consist of 273 and 260 amino acids. A sequence comparison between the subunits of TR-I and TR-II has shown that they share 167 (64 %) identical residues (Nakajima *et al*., 1993) (Figure 1-2). The amino-terminal halves

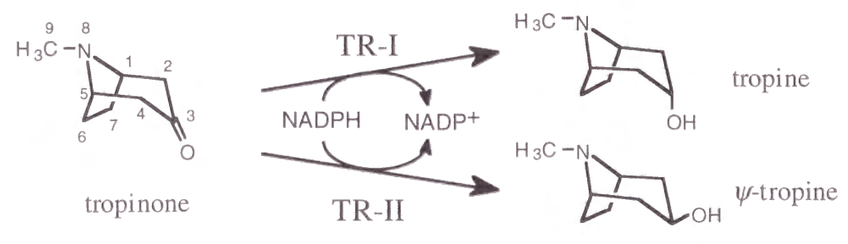

Figure 1-1. Reaction of tropinone reductases (TRs).

```
                                10        20        30        40
tr1         MEESKVSMMNCNNEGRWSLKGTTALVTGGSKGIGYAIVEELAGLGARVYTCSRNEKELDE
tr2         ------------MAGRWNLEGCTALVTGGSRGIGYGIVEELASLGASVYTCSRNQKELND
                        ***.*:* ********:****.******.*** *******:***::

            50        60        70        80        90        100
tr1         CLEIWREKGLNVEGSVCDLLSRTERDKLMQTVAHVFDGKLNILVNNAGVVIHKEAKDFTE
tr2         CLTQWRSKGFKVEASVCDLSSRSERQELMNTVANHFHGKLNILVNNAGIVIYKEAKDYTV
            **  **.**::**.***** **:**::**:***: *.***********:**:*****:*

            110       120       130       140       150       160
tr1         KDYNIIMGTNFEAAYHLSQIAYPLLKASQNGNVIFLSSIAGFSALPSVSLYSASKGAINQ
tr2         EDYSLIMSINFEAAYHLSVLAHPFLKASERGNVVFISSVSGALAVPYEAVYGATKGAMDQ
            :**.:**. ******** :*:*:****:.***:*:**::*  *:*  ::*.*:***::*

            170       180       190       200       210       220
tr1         MTKSLACEWAKDNIRVNSVAPGVILTPLVETAIKKNPHQKEEIDNFIVKTPMGRAGKPQE
tr2         LTRCLAFEWAKDNIRVNGVGPGVIATSLVEMTIQ-DPEQKENLNKLIDRCALRRMGEPKE
            :*:.** **********.*.**** *.*** :*: :*.***:::::* : .: * *:*:*

            230       240       250       260
tr1         VSALIAFLCFPAASYITGQIIWADGGFTANGGF     (273)
tr2         LAAMVAFLCFPAASYVTGQIIYVDGGLMANCGF     (260)
            ::*::**********:*****:.***: ** **
```

Figure 1-2. Comparison of the amino acid sequences of TR-I and TR-II. The amino acid sequences of TR-I and TR-II from *D. stramonium* were aligned with CLUSTAL W (Higgins *et al.*, 1992) using default parameters. The numbering at the top is according to the numbering of the sequence of TR-II. Amino acid sequences are shown in single-letter code. Hyphens, asterisks, colons and dots indicate gaps, identical residues, strongly functionally conserved residues, weakly functionally conserved residues, respectively. Residues that are highly conserved in SDRs (Jörnvall *et al.*, 1995) are shown in black boxes.

show higher homology (72 % identical) than the carboxyl-terminal halves (57 %). The results obtained from the analyses of chimeric TR enzymes have indicated that the carboxyl-terminal peptides containing approximately 120 amino acid residues (in TR-II, from Glu120 to Ala239) participate in the stereospecificity and the substrate specificity for cyclic carbonyl substrates (Nakajima *et al.*, 1994).

The amino acid sequences of the TRs have also indicated that the enzymes belong to the short-chain dehydrogenase/reductase (SDR) family (Nakajima *et al.*, 1993; Jörnvall *et al.*, 1995). The SDR family shows distinctive properties from the classical yeast/liver alcohol dehydrogenase and related enzymes, termed the medium-chain dehydrogenase/reductase (MDR) family. Typical MDR family enzymes consist of subunits with 350 - 375 residues, and very often include zinc ions. In zinc-containing MDR enzymes, cysteine residues coordinate zinc ions at the active site. The enzymatic mechanisms and the three-dimensional structures of the enzymes of this family have been studied extensively, with the first three-dimensional structure determined in the early 70's (Boyer, 1975). On the other hand, the group of SDR family has

been identified relatively recently (Jörnvall *et al.*, 1981). The SDR family enzymes have fewer number of residues, from 241 to 327, but exhibit sequence identities only at 15 - 30 % level among them. The enzymatic reactions do not depend on metals or cysteine thiols. In the SDR family, a Tyr-X-X-X-Lys segment is strictly conserved. The tyrosine residue has been identified as a crucial component of the enzymatic function based on the results from the chemical modifications and site-directed mutagenesis (Ensor and Tai, 1991; Obeid and White, 1992; Chen *et al.*, 1993; Cols *et al.*, 1993; Kiefer *et al.*, 1996; Kiefer *et al.*, 1997; Liu *et al.*, 1997). The functions of the conserved residues (tyrosine, lysine, and in addition, serine) has been proposed from the three-dimensional structures of the SDR enzymes which have been determined in the 90's for the first time (Ghosh *et al.*, 1994; Ghosh *et al.*, 1995; Rafferty *et al.*, 1995; Andersson *et al.*, 1996; Azzi *et al.*, 1996; Breton *et al.*, 1996; Tanaka *et al.*, 1996a; Tanaka *et al.*, 1996b). That is, the tyrosine acts as a general acid/base catalyst, and the lysine and the serine facilitate this function through electrostatic effects and hydrogen bonding with the tyrosine, respectively. These residues are also conserved in TR-I and TR-II (Figure 1-2), therefore it is presumed that the reaction mechanism common to the SDR enzymes is shared by the two TRs.

Taking into account the results so far, both TRs seem to have a common reaction mechanism but have different reaction stereospecificities. Therefore, it is of great interest to elucidate the structural basis for their stereospecific reaction mechanisms. Several attempts to understand the reaction stereospecificity using structural analysis have been reported (Lamzin *et al.*, 1995). In NAD(P)-dependent enzymes, structures of formate dehydrogenase (FDH), D-glycerate dehydrogenase (D-GDH) and D-lactate dehydrogenase (D-LDH) were compared with those of L-LDH or L-malate dehydrogenase (Goldberg *et al.*, 1994; Lamzin *et al.*, 1994a; Lamzin *et al.*, 1994b; Stoll *et al.*, 1996). The results showed that they have no overall structural relationships but have convergence of the active site residues, which were related by a mirror plane (in FDH case), a rotation (in D-GDH case) with respect to L-specific enzymes. D-LDH also shows the convergence, though it has different chemical nature of the active site from that of L-LDH. In contrast, the TRs have high sequence similarity even though they have opposite stereospecificity. Therefore, it is expected that the TRs might posses a new structural basis for controlling stereospecificity in the reaction.

In this study, the author has aimed to elucidate the structural basis for the stereospecific reaction mechanism of TRs. To this end, the author has carried out X-ray crystallographic analysis of TR-II. Structure determination of TR-I has also been performed independently by

Professor Yamada and his coworkers at Nara Institute of Science and Technology. The comparison of the TR-I structure with the TR-II structure determined in this thesis has identified factors which differentiate their stereospecificities. CHAPTER 2 describes the purification and crystallization of TR-II from *D. stramonium*, and its preliminary X-ray crystallographic analysis. CHAPTER 3 describes the three-dimensional structure of TR-II at 2.3 Å resolution which was determined for the first time using the multiple isomorphous replacement method. The resulting TR-II structure has allowed one to compare the TR-I structure, and to propose the factors important in maintaining the stereospecificity. This was further advanced by the crystallographic structure of a TR-II ternary complex with $NADP^+$ and ψ-tropine at 1.9 Å resolution, which is described in CHAPTER 4. The refined structure of the ternary complex has revealed the substrate binding mode responsible for stereospecific reaction. The active site architecture has also given insights into the catalytic mechanism of the enzyme.

CHAPTER 2

Crystallization and Preliminary Crystallographic Study of Tropinone Reductase-II

2-1. Introduction

Crystallographic structure determination begins with growth of suitable crystals. First of all, it is essential to develop a purification process which can produce a large amount of highly purified protein for crystallization. Next, extensive search of crystallization condition is needed. Producing appropriate crystals often requires both initial screening and subsequent optimization. Screening relies on uniform, randomized sampling to identify combinations of variables that give rise to crystalline lattices. Optimization involves adjusting the conditions identified by screening so as to improve the crystals. If optimization to obtain sufficiently large single crystals is not successful, then a seeding technique can be tried, in which micro crystals are transferred from the solution in nucleation conditions to those that will support only crystal growth (Thaller *et al.*, 1985; Stura and Wilson, 1990).

If a sufficiently large single crystal can be obtained, quality of the crystal must be checked by X-ray diffraction experiments, since crystallographic structure analysis requires accurately measured diffraction intensity data of the crystal. However, diffractions from protein crystals are often rather weak especially at high resolution, and are liable to suffer from radiation damage by X-ray. One of the most effective way to overcome these problems during data collection, especially the radiation damage, is application of cryocrystallography (Hope, 1988; Hope, 1990; Watenpaugh, 1991; Rodgers, 1994; Rodgers, 1997). The primary benefit of data collection at cryogenic temperature is a reduction in the rate of radiation damage, which often substantially extends crystal lifetime. Furthermore, in many cases, the high resolution to which accurate data can be recorded increases, either because of a reduction in thermal disorder or simply as a result of longer exposure times and a more stable crystal. In addition, low-temperature techniques can be used to stabilize transient states, such as catalytic intermediates, that are too short-lived for study at higher temperatures (Moffat and Henderson, 1995). However, there are number of cases where it is very difficult to freeze crystals without causing unacceptable lattice distortion or an increase in the mosaicity of the crystals.

When crystals are cooled to cryogenic temperature, it is necessary to prevent formation of

crystalline ice inside and outside of the crystals, which causes lattice distortion. The most effective and generally applicable technique to cool crystals is a flash-cooling technique. That is, the temperature of a crystal is rapidly lowered to -180 ~ -150 ˚C in order to reach below the glass transition temperature before ice-crystal nucleation occurs. In order to slow the nucleation of ice and raise the viscosity of the solution, cryoprotectant is generally added before flash-cooling (Petsuko, 1975). Cryoprotectants reported as useful so far are alcohols, sugars etc., such as glycerol, ethylene glycol, polyethylene glycol (PEG) 400, glucose and 2-methyl-2,4-pentanediol (MPD) (Rodgers, 1994; Rodgers, 1997). Composition and concentration of cryoprotectant need to be optimized for each protein sample or each crystallization condition. In addition, a novel crystal-mounting technique for flash-cooling was developed, in which the crystal is suspended in a film of mother liquor formed in a small loop (Teng, 1990). This method achieves high cooling rate and reducing back ground scatter and absorption, therefore is now generally used.

This chapter describes the purification and crystallization of TR-II. X-ray diffraction data collection using cryocrystallographic techniques and determination of crystallographic data were also described. Optimizing the crystallization condition and establishing a data collection method has allowed one to obtain a suitable dataset for the structure determination of TR-II.

2-2. Experimental Procedures

Materials

Plasmid pETTR2, constructed by subcloning of *Datura stramonium* TR-II cDNA into pET21d (Novagen; Madison, USA), was generously provided by Professor Y. Yamada, Nara Institute of Science and Technology, Japan. Tropinone was purchased from Aldrich (Milwaukee, USA). β-NADPH and β-$NADP^+$ were purchased from Oriental Yeast Co., Ltd. (Tokyo, Japan). 2-Methyl-2,4-pentanediol (code No. 68340) and ammonium dihydrogen phosphate (code No. 09709) for crystallization were purchased from Fluka (Buchs, Switzerland). 2-Propanol (specially prepared reagent: code No. 162-17001) for crystallization was purchased Wako Pure Chemical Industries (Osaka, Japan). All reagents were purchased at highest commercial quality and used without further purification.

Overproduction

Overproduction was carried out according to the method of Nakajima (Nakajima, 1997). *Escherichia coli* strain BL21(DE3) (Novagen) was transformed with the plasmid pETTR2 by the method of Hanahan (Hanahan, 1983). Transformants were grown first in 3 ml, then in 100 ml LB medium (1 % bacto-tryptone, 0.5 % bacto-yeast extract, 1 % NaCl, pH 7.5) containing 200 μg/ml ampicillin at 37 ˚C with vigorous shaking until the culture reached at a log phase (A_{600} = 0.7 - 1.0 cm^{-1}). This 100 ml-culture was then transferred to a total 5 L of the same medium and again incubated at 37 ˚C with vigorous shaking (300 rpm). Isopropyl-β-D-thiogalactopyranoside was added to a final concentration of 1 mM at the log phase, followed by culturing at 25 ˚C with mild shaking (100 rpm) for 16 hours. Bacteria were harvested, washed once with 20 mM Tris-HCl (pH 7.0) containing 150 mM NaCl, and suspended in buffer A [100 mM potassium-phosphate (pH 7.0), 3 mM dithiothreitol (DTT)] supplemented with 10 μg/ml lysozyme and 0.1 % (v/v) Triton X-100. The cells were lysed by three rounds of freezing-thawing cycle, followed by sonication at 0 ˚C. Cell-free extract was recovered by centrifugation at 10,000 × *g* for 20 min at 4 ˚C.

Purification

All the following procedures were performed at 4 ˚C. The cell-free extract was diluted to protein concentration of 5 mg/ml with buffer A (described above), and the TR-II fraction was precipitated with ammonium sulfate between 40 and 75 % saturation. The precipitant was dissolved in buffer B [20 mM potassium-phosphate (pH 7.0), 5 mM ethylenediamine tetraacetic acid (EDTA), 1 mM DTT and 10 % (v/v) glycerol] containing 40 % saturated ammonium sulfate. The solution was applied to a Phenyl Sepharose 6 Fast Flow column (Pharmacia Biotech; Uppsala, Sweden; 2.6 ϕ × 38 cm) equilibrated with buffer B containing 40 % saturated ammonium sulfate. After washing the column with 400 ml of the same buffer, elution was done with a linear gradient from 40 % (900 ml) to 0 % (900 ml) ammonium sulfate saturation in buffer B. The active fraction was eluted at an ammonium sulfate concentration of approximately 10 % saturation. The active fraction was concentrated on a YM-10 membrane (Amicon; Beverly, USA), dialyzed against buffer B, then applied to a 2',5'-ADP Sepharose 4B column (Pharmacia Biotech; 2.6 ϕ × 11 cm) equilibrated with buffer B. The column was washed with 120 ml of buffer B, and then eluted with a linear KCl gradient from 0 M (300 ml) to 0.8 M (300 mL) in buffer B. The active fraction was concentrated and dialyzed against buffer C [50 mM Tris-HCl (pH 7.5), 5 mM EDTA, 1 mM DTT and 10 % (v/v) glycerol]. The retentate was then applied to a DEAE Cellulofine A-800 column (Chisso; Tokyo, Japan; 2.6 ϕ ×

19 cm) equilibrated with buffer C. Finally the purified protein was eluted by washing the column with buffer C.

The course of purification was monitored by sodium dodecylsulfate polyacrylamide-gel electrophoresis (SDS-PAGE) (Laemmli, 1970). The purified protein solution was dialyzed against 5 mM Tris-HCl (pH 7.4) with 1 mM DTT, and was concentrated to 7.5 or 15.0 mg/ml using a YM-10 membrane and Centricon-10 (Amicon), then stored at -80 ˚C.

Measurement of TR-II Activity

Protein concentration was measured using the method of Bradford (Bradford, 1976) with Protein Assay Reagent (Pierce Chemical Co.; Rockford, USA), and bovine serum albumin was used as a standard. The activity of TR-II was assayed spectrophotometrically by monitoring the change in the absorbance of NADPH at 340 nm using a molar absorption coefficient of 6200 $M^{-1}cm^{-1}$. A solution of TR-II (50 µl) was added to an assay medium consisted of 4 mM tropinone, 0.2 mM NADPH and 0.1 M potassium-phosphate (pH 5.9) in a total volume of 1 ml, and the course of the reaction was monitored at 37 ˚C.

Crystallization

The crystallization conditions were screened by a revised sparse-matrix method (Jancarik and Kim, 1991; Cudney *et al*., 1994), using Crystal Screen I and II (Hampton Research; Laguna Hills, USA). Crystals were grown in a 24 well Multiwell Tissue Culture Plate (Becton Dickinson Labware; Lincoln Park, USA) using the hanging-drop vapor diffusion method at 20 ˚C. Each drop contained 2 µl of the protein solution and 2 µl of the reservoir solution.

Macro-seeding technique was used in order to obtain larger crystals (Thaller *et al*., 1985; Stura and Wilson, 1990). In this case, crystals were grown in a CRYSCHEM MVD/24 plate (Supper; Natick, USA) using the sitting-drop vapor diffusion method. A drop contained 5 µl of the protein solution and 5 µl of the reservoir solution, and was equilibrated with the reservoir solution for 1-2 days prior to transfer of a seed crystal. Seed crystals prepared in the hanging-droplets were washed once with the same solution as the reservoir but contained the ligand and slightly lower (*ca.* 90 %) concentration of the precipitant. After being transferred to the sitting-drops, the seed crystals were allowed to grow at 20 ˚C.

X-ray Diffraction Experiments

X-ray diffraction data were collected either at room temperature from a crystal mounted in a thin-walled glass capillaries, or at -160 ˚C in a stream of nitrogen generated by a Sample Spray-

cooling Unit (Rigaku; Tokyo, Japan). Just before the data collection at the cryogenic temperature, the crystals were mounted in nylon mono-fiber loops and flash-frozen by plunging them into liquid nitrogen (Teng, 1990; Rodgers, 1994; Rodgers, 1997). Nylon loops were made using Cryo-Loop Kit (Supper) and attached to CrystalCap System (Hampton Research).

Precession photographs were taken with Ni-filtered Cu $K\alpha$ radiation from an RU-300 rotating anode (Rigaku) operated at 40 kV and 100 mA, using Buerger precession goniometer (Huber; Rimstng, Germany). The distance between the crystal and the detector was 100 mm, and the precession angle was set to 15 degrees.

Diffraction intensity data were collected on an R-AXIS IIc imaging-plate area detector (Rigaku) with monochromatized Cu $K\alpha$ radiation from the same rotating anode operated at 40 kV and 100 mA. Data were reduced using the program PROCESS (Sato *et al.*, 1992).

2-3. Results and Discussion

Purification of TR-II

The TR-II expressed in *E. coli* was extracted and fractionated with ammonium sulfate of 40-75 % saturation. TR-II was then purified using three chromatographies; Phenyl Sepharose as a hydrophobic chromatography, 2',5'-ADP Sepharose as an affinity chromatography, and DEAE Cellulofine as an ion-exchange chromatography. Since TR-II is an NADPH dependent enzyme, 2',5'-ADP was chosen as a ligand for the affinity chromatography. It worked

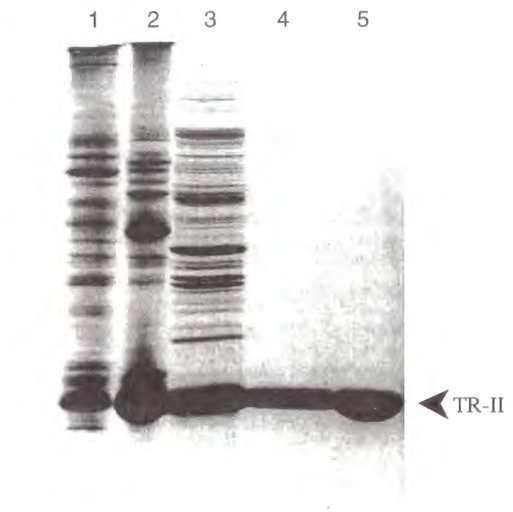

Figure 2-1. SDS-PAGE analysis of enzyme purification. 12.5 % polyacrylamide gel was used. Lane 1, crude extract; lane 2, 40-75 % ammonium sulfate fraction; lane 3, Phenyl Sepharose fraction; lane 4, 2',5'-ADP Sepharose fraction; lane 5, DEAE Cellulofine fraction.

Table 2-1. Purification of TR-II.

Purification steps	Total protein (mg)	Total activity (mKat[a])	Yield (%)	Specific activity (nKat[a]/mg)	Purity (-fold)
Crude extract	1480	105	100	70.9	1.0
40-75 % $(NH_4)_2SO_4$	574	58.3	55.5	101.6	1.4
Phenyl Sepharose	248	55.4	52.8	223.4	3.1
2',5'-ADP Sepharose	90.6	31.2	29.7	344.1	4.9
DEAE Cellulofine	60.2	22.7	21.6	377.5	5.3

[a]One katal of enzyme was defined as the amount that reduced the 1 mol of tropinone per second.

effectively in this purification process. The sample after this purification procedure was homogeneous judged by SDS-PAGE (Figure 2-1), and used in subsequent crystallization. The results of the purification are summarized in Table 2-1.

Crystallization of TR-II

In preliminary screening of crystallization conditions, TR-II crystals were obtained under two different conditions with and without $NADP^+$ using polyethylene glycol (PEG) 6000 and ammonium acetate as a precipitant (Table 2-2) (Nakajima, 1997). The crystals grew to a typical size of $0.3 \times 0.3 \times 0.1$ mm within several days (Figure 2-2a).

X-ray analyses of these crystals were attempted. Unit-cell dimensions and the space group were determined from precession photographs (Figure 2-2b, Table 2-2). However, the diffraction spots from the crystals streaked along the c^* axis seriously (Figure 2-5a). This results indicated that these crystals had a strong anisotropic mosaicity along the c axis. Due to the poor diffraction quality, no further investigation of these crystals was pursued.

After searching other crystallization conditions, new crystals were obtained in the presence of tropinone using MPD as a precipitant (Table 2-3). The crystals grew to a typical size of $0.1 \times 0.1 \times 0.01$ mm within a week in hanging droplets. Subsequently, these crystals were used for the seeding techniques as macroseeds. At first these crystals were transferred to a solution containing 0.1 M 2-morpholinoethanesulfonic acid (MES) pH 6.0, 38 % (v/v) MPD, 0.2 M $NH_4H_2PO_4$ and 135 mM tropinone for several minutes in order to melt the

Table 2-2. Crystallization conditions and crystallographic parameters found in preliminary screening (modified from Nakajima(1997)).

	(Condition 1)	(Condition 2)
Protein solution	7.5 mg/ml TR-II 4 mM $NADP^+$	7.5 mg/ml TR-II
Reservoir solution	50 mM Na-citrate (pH 4.5) 9 % (w/v) PEG6000 0.28 M CH_3COONH_4 1 mM DTT 0.02 % (w/v) NaN_3	50 mM Na-citrate (pH 5.3) 6 % (w/v) PEG6000 7 % (v/v) 2-propanol 1 mM DTT 0.02 % (w/v) NaN_3
Crystal system	Tetragonal	
Space group	$P4_222$	
Cell parameters(Å)	$a = b = 63.3^a$ $c = 145.3^a$	
V_m (Å^3 Da^{-1})	2.60	
V_{solv} (%)	52.7	

[a]Determined at room temperature.

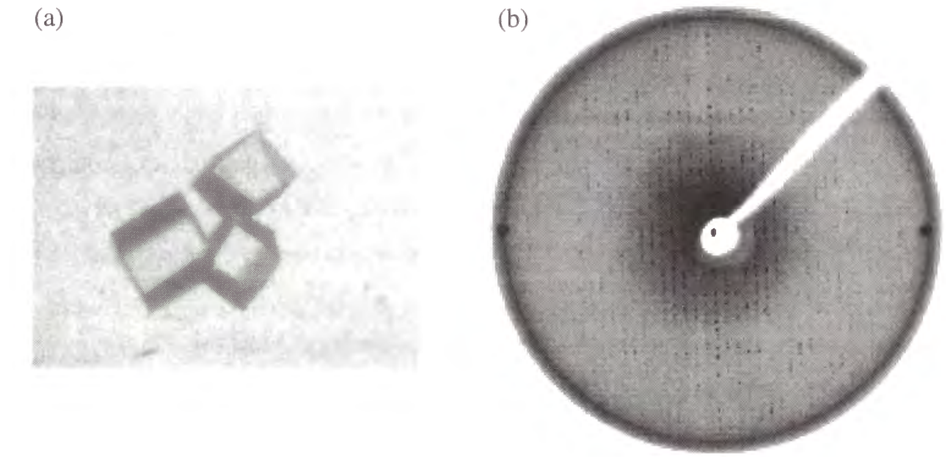

Figure 2-2. (a) TR-II crystals from condition 2 in Table 2-2. (b) A precession photograph of (h 0 l) plane of a TR-II crystal from condition 1 in Table 2-2.

Table 2-3. Crystallization condition of TR-II obtained from MPD.

Protein solution[a]	15 mg/ml TR-II 135 mM tropinone
Reservoir solution[a]	0.1 M MES (pH 6.0) 42 % (v/v) MPD 0.21 M $NH_4H_2PO_4$ 1 mM DTT 0.02 % (w/v) NaN_3

[a] 2 µl for making a hanging drop, 5 µl for making a sitting drop (in macroseeding method).

Figure 2-3. TR-II crystal from the condition in Table 2-3.

crystal surface slightly, then transferred to a 10 µl of solution which has the same composition of the hanging droplets to be allowed to grow. The crystals grew to a typical size of $0.5 \times 0.5 \times 0.05$ mm within several weeks (Figure 2-3). Tropinone was necessary for the crystal growth.

X-ray Diffraction Data Collection using Flash-Cooling Method

The X-ray analysis of the newly-obtained crystals was carried out. The crystals gave suitable diffraction for intensity measurements at room temperature, and streak of the diffraction spots was not observed. However, when the stock solution using PEG400 instead of MPD was added to the crystal prior to the data collection, the anisotropic increase of the mosaicity along the c^* axis (similar to the TR-II crystals from PEG6000) was again observed (data not shown). These results suggest that PEG causes disorder of the TR-II crystals.

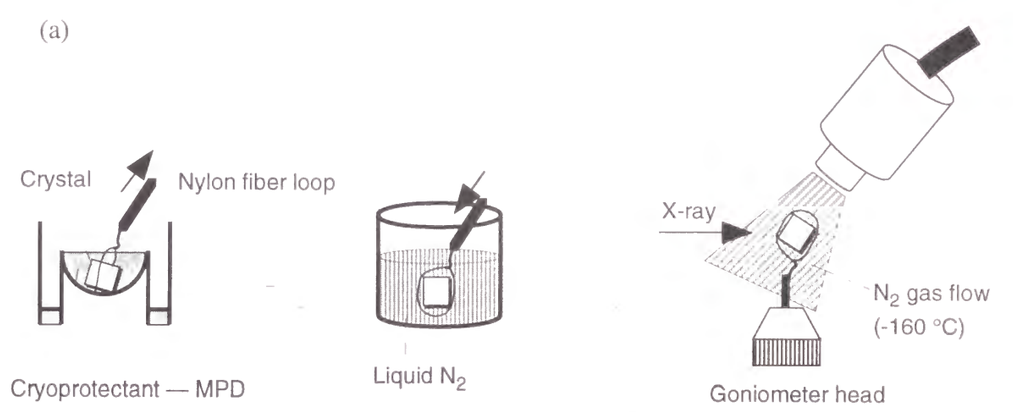

Figure 2-4. Flash-cooling method. (a) Schematic illustration of flash-cooling method. First, a crystal was picked up by a nylon fiber loop of 20 µm diameter, and was plunged into liquid nitrogen and frozen. Then the crystal was transferred into a 160 °C nitrogen flow immediately, and diffraction data were collected. (b) A TR-II crystal mounted on a nylon fiber loop and flash-frozen.

These TR-II crystals, however, were rather unstable under the conventional X-ray data collection condition at room temperature, and it was difficult to collect a complete diffraction dataset. Therefore, diffraction data collection was carried out at a cryogenic temperature (-160 °C) by flash-cooling the crystals in the following way (see Figure 2-4). The crystals were first transferred to a stock solution containing 0.1 M MES pH 6.0, 50 % (v/v) MPD, 0.2 M $NH_4H_2PO_4$ and 135 mM tropinone, then flash-frozen in liquid nitrogen. MPD in the stock solution served as an effective cryoprotectant. A 20 µm diameter nylon mono-fiber was used to make loops for picking up crystals. This thickness was chosen since it was easier to manipulate

than thinner loops such as 10 μm diameter. Fiber diffractions from the loop made of the 20 μm diameter nylon mono-fiber were negligible. As the cooling method, in the case of TR-II, plunging crystals into liquid nitrogen was effective to prevent the increase of the crystal mosaicity rather than putting the crystals into the nitrogen flow directly. As a result, it became possible to keep a TR-II crystal stable during data collection. The crystals also gave suitable diffraction for intensity measurement under the cryogenic condition (Figure 2-5b). Moreover, this method reduced the diffraction damage by X-ray effectively. Decay of diffraction intensity was not observed at all during data collection for more than 25 hours under the cryogenic condition (Figure 2-6).

Crystallographic Data of TR-II Crystals

Unit-cell dimensions and the space group were determined using the autoindexing routine and the simulated precession in the program PROCESS (Sato *et al*., 1992) (Table 2-4). The space group was assigned as $P4_22_12$ by the $P4$/mmm laue symmetry and the systematic absence of h = 2n+1 for $h00$ reflections and l = 2n+1 for $00l$ reflections of the diffraction data. The volume-to-mass ratio (V_m) and the solvent content of the crystal were calculated assuming one protein subunit per asymmetric unit (Table 2-4). These values are reasonable compared to those normally found in protein crystals (Matthews, 1968). The intensity data were collected to a resolution of 2.0 Å using an R-AXIS IIc. The data were scaled and merged to yield a completeness of 81.8 % to 2.0 Å resolution with an R_{merge} of 8.74 %. Data collection statistics are summarized in Table 3-2 as "Native". The diffraction data obtained from these TR-II crystals was shown to be suitable for structure determination. Further X-ray analysis was carried out using these crystals.

Table 2-4. Crystallographic data of TR-II.

Crystal system	Tetragonal
Space group	$P4_22_12$
Cell parameters(Å)	$a = b = 62.8$ Å, $c = 128.4$ Å $\alpha = \beta = \gamma = 90$ °
V_m (Å^3 Da^{-1})	2.24
V_{solv} (%)	45.0 %

(a)

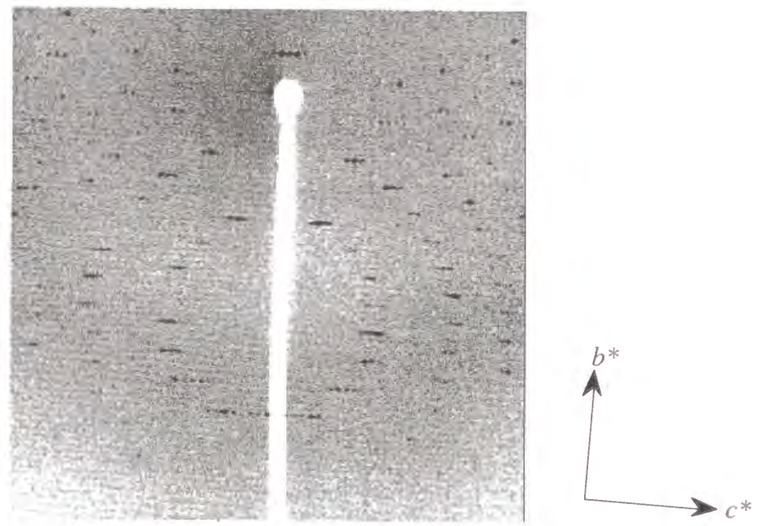

(b)

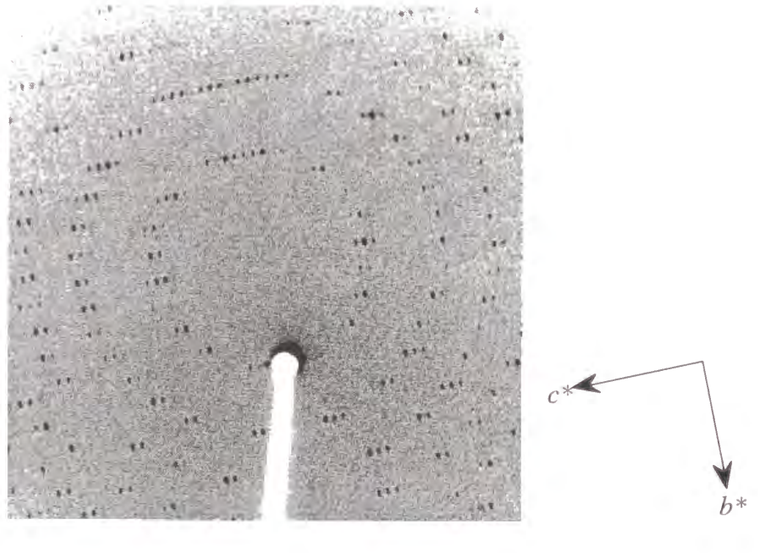

Figure 2-5. (a) An oscillation photograph of a TR-II crystal from condition 2 in Table 2-2. The diffraction pattern was obtained with an R-AXIS IIc imaging-plate at room temperature. Rigaku rotating anode was operated at 40 kV and 100 mA. The crystal to detector distance was 140 mm, the oscillation angle was 1.2 °, and the exposure time was 30 min. The a*-axis tilted 37 ° from the direction of the X-ray beam. The white zone in the figure is a shadow of the beam stopper. (b) An oscillation photograph of a TR-II crystal from the condition in Table 2-3. The diffraction pattern was obtained at -160 °C. the exposure time was 18 min. The a*-axis tilted 28 ° from the direction of the X-ray beam. Other conditions were the same as described in (a).

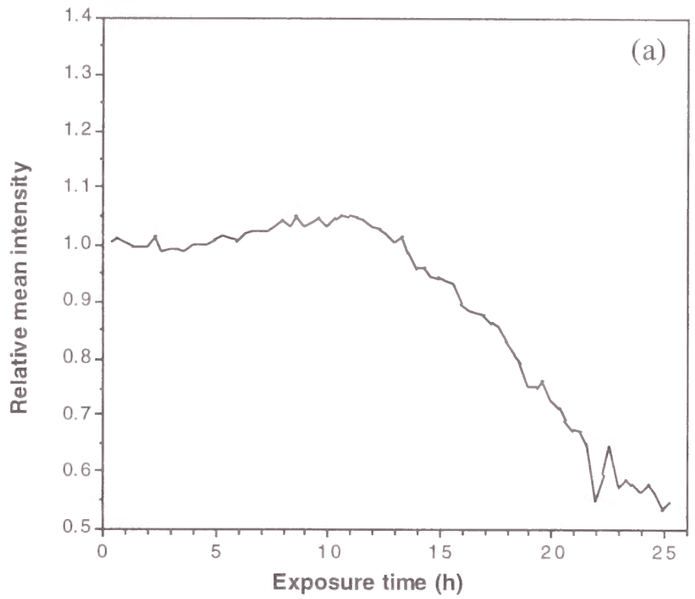

Figure 2-6. Comparison between diffraction intensity of a TR-II crystal at room temperature and at cryogenic temperature (-160 °C). Seventy-six flames of oscillation photograph were taken with 1.2 ° oscillation angle. Mean intensity of each flame *vs.* the time when the exposure of the flame finished was plotted. Intensity was represented as relative value to the first flame, which was set to 1.0. Rigaku rotating anode was operated at 40 kV and 100 mA and the diffraction intensities were detected with R-AXIS IIc. The crystal to detector distance was 140 mm. X-ray was incident along c^* axis direction at the first flame, and along a^* axis direction at the last flame. (a) At room temperature. The crystal size was $0.3 \times 0.3 \times 0.1$ mm. (b) At -160 °C. The crystal size was $0.36 \times 0.36 \times 0.1$ mm.

CHAPTER 3

Crystal Structure of Tropinone Reductase-II

3-1. Introduction

Crystallographic structure determination involves building a structure model based on electron density maps calculated from diffraction intensity data. Obtained diffraction data, however, contain only the amplitudes of the diffracted waves from a crystal. To reconstruct a map of electron density in the crystal, the unmeasured phase information is also required.

The most general technique for determining protein phase angles is the multiple isomorphous replacement (MIR) method, if no three-dimensional structure information of the protein, such as a structure of a homologous protein, is available (Green *et al*., 1954; Drenth, 1994). This method requires at least two heavy atom derivative crystals, in which heavy atoms are bound to specific sites of protein molecules. Suitable derivative crystals for phase determination are that have a small number of heavy atom binding sites with high occupancies, and the crystals should be isomorphous to the native crystal. Obtaining such derivative crystals requires extensive screening of the conditions with different heavy atom reagents. If diffraction data of the native and derivative crystals can be collected successfully, the positions of the heavy atoms are determined from the Patterson functions (Patterson, 1934). Then the protein phases can be calculated using these heavy atom positions.

Since initial phases generally include some errors which often introduce noises in electron density maps, phase improvement is necessary. A widely used method for phase improvement is solvent flattening (Wang, 1985), which estimates the boundaries of the protein molecules and set electron density between them to a low constant value. If there is a noncrystallographic symmetry within the asymmetric unit, molecular averaging is also useful (Bricogne, 1976). In some cases, a significant fraction of the structure can be reliably determined from an electron density map, but some regions in the map might be less well defined. In such cases, it is often effective to combine the phase information from the well defined parts of the structure with the MIR phases. When making use of partial structure information, however, the resulting phases are always biased towards the partial structure. In order to minimize such bias, Read (Read, 1986) has proposed two procedures: (1) how to apply proper weights to the phases derived from the partial structure when combining them with phases derived from other means, and (2)

how to calculate maps using the partial structure phases. In the former procedure, phases are combined using σ_A weighting, which is a combined measure of the completeness and the accuracy of the partial structure:

$$\sigma_A = D\,(\varepsilon|F_P|^2 / \varepsilon'|F_N|^2)^{1/2}$$

$D = \langle\cos(2\pi s.\Delta r)\rangle$, where Δr indicates positional errors.

F_P, F_N: structure factors of the partial structure and native structure, respectively.

ε, ε': correction factors for expected intensity in reciprocal-lattice zone.

In the latter procedure, in order to suppress the model bias, Fourier coefficients $(2m|F_o| - D|F_c|)\exp(i\alpha_c)$ and $(m|F_o| - D|F_c|)\exp(i\alpha_c)$ are used for calculating the electron density maps instead of conventional $(2|F_o| - |F_c|)$ or $(|F_o| - |F_c|)$ maps. (m (figure of merit) = $\langle\cos\Delta\varphi\rangle$, where $\Delta\varphi$ indicates phase error of the current model.)

After the structure models of the protein are built based on the electron density, refinement of the model is needed. Refinement is a process of adjusting the model to find a closer agreement between the calculated and observed structure factors. Conventional structure refinement is based on a least-squares minimization. Especially, simulated annealing method using molecular dynamics is a more effective minimization protocol than gradient methods (Brünger *et al*., 1987). However, if there is an error in the model that is outside the range of convergence of the refinement method, the least squares minimization method might lead to a better, but misleading, agreement in the amplitudes by introducing additional errors in the rest of the structure. As a result, the model accuracy is overestimated, and most of the model bias remains in the structure. To overcome this refinement bias problem, it is useful to use a maximum likelihood method based on probability distribution, since this method will not force the calculated structure-factor amplitudes to be equal to the observed amplitudes but lead to the assignment of the highest conditional probability (Read, 1990; Bricogne, 1991). In some cases the maximum likelihood method can be more effective compared to least-squares refinement (Murshudov *et al*., 1997).

This chapter describes the structure determination of TR-II using the MIR method. In this process, it was also necessary to use several of the phase improvement methods and the structure refinement methods described above. This is the first time that the three-dimensional structure of TR-II have been determined. The resulting TR-II structure has shown striking similarity to the TR-I structure, but has several different polar residues at the active site. These

residues have been proposed to be responsible for the difference of stereospecificities between TR-II and TR-I.

3-2. Experimental Procedures

Materials

K_2PtCl_4, K_2PtCl_6, $K_2Pt(CN)_4$, $K_2Pt(NO_2)_4$ and Platinum bis(ethylenediamine)chloride (*cis*-$PtCl_2$) were purchased from Aldrich. $KAu(CN)_2$, $HgCl_2$, CH_3HgCl, C_2H_5HgCl, CH_3COOHg, $Hg(CH_3COO)_2$ and phenylmercury acetate (PheAceHg) were obtained from Wako Pure Chemical Industries, Ltd. $Sm_2(SO_4)_3$, $NaAuCl_4$, $Pb(CH_3COO)_2$, K_2HgI_4 and CH_3COOTl were purchased from Nacalai Tesque (Kyoto, Japan). Na_3IrCl_6 and ethylmercurithiosalicylic acid sodium salt (EMTS) were purchased from Katayama Chemical (Osaka, Japan). *p*-Chloromercuri benzene sulfonic acid sodium salt (PCMBS) were obtained from Sigma (St. Louis, USA). Ethylmercuri phosphate (EMP) was a gift from Professor G. A. Petsuko at Brandies University, U.S.A. All reagents were purchased at highest commercial quality and used without further purification.

N-Terminal Amino Acid Sequence Analysis

TR-II protein prepared as described in CHAPTER 2 was further purified by SDS-PAGE. The purified TR-II was blotted on polyvinylidene difuluoride membrane (Immobilon Transfer Membrane; Millipore; Bedford, USA) by electroblotting method (Vendekerckhove *et al.*, 1985). Edman degradations were performed automatically using a gas-phase peptide sequencer (Applied Biosystems Model 477A) linked with a phenylthiohydantoin analyzer (Applied Biosystems Model 120A). The 3-phenyl-2-thiohydantoin amino acid derivatives were identified with high performance liquid chromatography.

Preparation of Heavy Atom Derivative Crystals

Heavy atom derivative crystals were prepared with a soaking method. The TR-II native crystals were prepared as described in CHAPTER 2. The native crystals were transferred twice to the stock solution [0.1 M MES pH 6.0, 50 % (v/v) MPD, 0.2 M $NH_4H_2PO_4$ and 135 mM tropinone] in order to remove DTT and NaN_3 used in the crystallization. Then the native crystals were soaked into the stock solution including a heavy atom reagent at 20 °C in the dark. The soaking conditions are summarized in Table 3-1.

Table 3-1. List of the compounds used for heavy atom derivatives.

Compound	Concentration (mM)[a]	Soaking time[b]	Comment
K_2PtCl_4	10 / 0.5 / 0.1	23.5 h / 52 h / 7 d	lack of isomorphism
K_2PtCl_6	saturated	2 d	lack of isomorphism
$K_2Pt(CN)_4$	2.0 / 1.0	5 d / 43 h	too many sites
cis-$PtCl_2$	1.0	60 h	too weak binding
$K_2Pt(NO_2)_4$	0.1	40 d	lack of isomorphism
$KAu(CN)_2$	3.0	2 d	too many sites
	1.0	6 d	useable¶
	0.5	4 d	too weak binding
$NaAuCl_4$	1.0 / 0.2	1 d / 4 d	crystal damage
EMTS	1.0	5 h	poor diffraction
	0.5 / 0.1 / 0.01	9 h / 13 h / 16.5 h	
PCMBS	1.0	5 d	crystal damage (crack)
	0.01	15 h	poor diffraction
$HgCl_2$	0.1	24 h	crystal damage
	0.1	8 h	useable¶
	0.05 / 0.01	8 h / 11.5 h	
CH_3HgCl	0.01 / 4 equiv.	5 h / 17.5 h	poor diffraction
C_2H_5HgCl	0.01 / 2 equiv	15.5 h / 16.5 h	poor diffraction
PheAceHg	2 equiv.	18 h	poor diffraction
K_2HgI_4	0.01	17 h	poor diffraction
EMP	0.01	16 h	poor diffraction
CH_3COOHg	0.5	21 h	poor diffraction
$Hg(CH_3COO)_2$	0.1	12 h	poor diffraction
	0.01	18 h	too many sites
$Pb(CH_3COO)_2$	1.0	2 d	crystal damage (crack)
	0.5	4 d	too weak binding
$Sm_2(SO_4)_3$	saturated	62.5 h	too weak binding
Na_3IrCl_6	1.0	17 d	lack of isomorphism
CH_3COOTl	1.0	5 d	lack of isomorphism

[a]"equiv." indicates mols of a heavy atom proportional to 1 mol of protein. [b]"h" and "d" indicate hours and days, respectively. ¶These compounds and soaking conditions were used for MIR phasing.

X-ray Diffraction Data Collection

X-ray diffraction data of the native crystal and heavy atom derivative crystals were collected at -160 °C using the flash-cooling method described in CHAPTER 2. The intensity data were collected on an R-AXIS IIc with RU-300 operated at 40 kV and 100 mA, and reduced with PROCESS. The data collection statistics used for phasing are summarized in Table 3-2.

Phase Determination

Phase determination was carried out using the MIR method (Green *et al*., 1954) supplemented with the anomalous scattering technique (Bijvoet, 1954) (MIRAS). Determination and refinement of the heavy atom parameters, and subsequent phase calculation and refinement described below were done using the PHASES software package (Furey and Swaminathan, 1997).

The heavy-atom sites of derivative crystals were determined from difference Patterson maps followed by the difference Fourier method (Patterson, 1934; Stryer *et al*., 1964). Two derivative crystals, a $KAu(CN)_2$-derivative and a $HgCl_2$-derivative (Table 3-2), were found to be suitable for phase calculation. The positions, occupancies and temperature factors of the heavy atoms were further refined using the program PHASIT with the conventional refinement method using the reflections with $F > 2\ \sigma(F)$ and the value of figure of merit > 0.3 in ∞ - 2.6 Å resolution range. Subsequent phase calculation was carried out using 8101 independent reflections with $F > 2\ \sigma(F)$ in ∞ - 2.6 Å resolution range. Both isomorphous and anomalous data of the Au-derivative and isomorphous data of the Hg-derivative up to 2.6 Å resolution were used, and anomalous data of the Hg-derivative up to 3.0 Å were used. The refined heavy atom parameters and the phasing statistics are shown in Table 3-3 and Table 3-4, respectively.

Phase Improvement and Model Building

The initial phase was improved using the solvent flattening protocol (Wang, 1985) with the DOALL procedure. The bulk solvent fraction was set to 43 %. Structure models were built with the program TURBO-FRODO (Bio-Graphics) in the region where electron density was readily recognizable. Phases of the partial models were calculated using PHASIT and combined with the MIR phase using BNDRY with σ_A weighting (Read, 1986). The cycle of model building and phase combination was repeated throughout the model-building step.

Table 3-2. Data collection statistics.

	Native1[a]	Native2[a]	$KAu(CN)_2$	$HgCl_2$
Soaking condition (conc., time)			1.0 mM 6 days	0.1 mM 8 hours
Camera length (mm)	140	140	140	140
2θ angle	0 °	10 °	0 °	0 °
Spindle axis	*+b**	*+b**	*+b**	*-a**
Oscillation angle	1.2 °	1.0 °	1.2 °	1.2 °
Exposure time (min./flame)	18	25	25	30
No. of flames	76	90	76	76
Resolution (Å)		2.0	2.6	2.6
No. of reflections				
Total ($I > \sigma(I)$)		103356	46382	52405
Unique ($I > \sigma(I)$)		14339	8069	8374
Completeness (%)				
Overall		81.8	94.8	97.7
Outer shell		55.0 (2.25 - 2.02 Å)	89.1 (2.75 - 2.60 Å)	93.6 (2.75 - 2.59 Å)
R_{merge}[b] (%)				
Overall		8.74	8.61	6.08
Outer shell		21.6 (2.25 - 2.02 Å)	19.6 (2.75 - 2.60 Å)	16.8 (2.75 - 2.59 Å)
R_{iso}[c] (%)			4.4	3.3
R_{ano}[d] (%)			2.5	1.3

[a]The Native data sets were collected with two different settings (2θ = 0° and 10°) using the same crystal, and merged by the program PROCESS.
[b]$R_{merge} = \sum\sum | \langle I_h \rangle - I_{h,i} | / \sum\sum I_{h,i}$, where $I_{h,i}$ and $\langle I_{h,i} \rangle$ are the ith intensity and the mean intensity of reflection h, respectively.
[c]$R_{iso} = \sum |F_{PH} - F_P| / \sum(F_{PH} + F_P)$, where $|F_{PH}|$ and $|F_P|$ are the structure factor amplitudes of the derivative and native crystals, respectively.
[d]$R_{ano} = \sum |F_{PH}(+) - F_{PH}(-)| / \sum(F_{PH}(+) + F_{PH}(-))$, where $F_{PH}(+)$ and $F_{PH}(-)$ represent the structure factor amplitudes for reflections ($h\ k\ l$) and ($-h\ -k\ -l$), respectively.

Structure Refinement

The structure models were refined with the program X-PLOR version 3.851(Brünger, 1992b) using the parameter set of Engh and Huber (Engh and Huber, 1991), and the program REFMAC (Murshudov *et al.*, 1997) in the CCP4 package(Collaborative Computational Project, No4, 1994). Six percent of the data was set aside for the calculation of the free *R*-factor (R_{free}), which was monitored during the refinement (Brünger, 1992a).

In the initial stage, the structure model was refined by the slow-cool protocol (Brünger *et al.*, 1990) followed by positional and overall temperature factor (B-factor) refinement using reflections with $F > 2\sigma(F)$ in 10 - 2.6 Å resolution range. SIGMAA style ($2m|F_o| - D|F_c|$) and ($m|F_o| - D|F_c|$) electron density maps (Read, 1986) were calculated using the PHASES package (Furey and Swaminathan, 1997), and used for rebuilding the structure model. Water molecules were included using the program WATERHUNTER (Sugio *et al.*, 1995). In the later stage, the model was refined with X-PLOR, followed by REFMAC using the 20 - 2.5 Å resolution range. In the refinement process with REFMAC, the maximum likelihood residual minimization method (Read, 1990; Bricogne, 1991) was used, and the overall B-factor refinement was also carried out. Map coefficients for SIGMAA style ($2m|F_o| - D|F_c|$)and ($m|F_o| - D|F_c|$) were also calculated using REFMAC, and these maps were used for model rebuilding. In the last stage, the model was refined by positional refinement and individual B-factor refinement using X-PLOR. The resolution was gradually increased to 2.3 Å during iteration of the refinement and rebuilding.

The stereochemical properties of the refined model were assessed using the program X-PLOR and PROCHECK (Laskowski *et al.*, 1993). The statistics of the model refinement are given in Table 3-6.

3-3. Results

Structure Determination and Refinement

Prior to the structure determination of TR-II, the N-terminal amino acid sequence analysis of the purified sample was carried out. The determined sequence was Ala-Gly-Arg-Trp-Asn-Leu-Glu-Gly-Cys-Thr, which matches to the sequence from Ala2 to Thr11 of TR-II. This result revealed that the N-terminal methionine was removed in TR-II protein purified from *E. coli.*

Structure determination of TR-II was carried out using the MIR method. First the

soaking conditions for preparing the derivative crystals were screened. Although most derivative crystals showed poor diffraction or lack of isomorphism (cell shrinkage) (Table 3-1), a $KAu(CN)_2$-derivative and a $HgCl_2$-derivative were found to be suitable for phase calculation. Thus diffraction data sets of the native crystal and these derivative crystals were collected under the cryogenic condition (Table 3-2). In general, derivative crystals tend to suffer from X-ray radiation damage and diffract weaker than native crystals. However, in the case of TR-II, data collection using cryocrystallographic technique yielded accurate intensity data even from the derivative crystals because of sufficient crystal stability and longer exposure times.

The difference Patterson maps calculated from these derivative data showed that there were two binding sites of the heavy atom in an asymmetric unit for both Au- and Hg-derivatives (Figure 3-1). On the other hand, the anomalous difference Patterson maps showed several peaks at positions similar to those of the isomorphous Patterson maps, but they were much weaker. The initial heavy atom positions were determined from the isomorphous difference Patterson maps. Then refinement of the heavy atom parameters was performed by an iterative method of phase determination and least squares refinement (Furey and Swaminathan, 1997). For phase calculation from the anomalous data of the Hg-derivative, diffraction data only up to 3.0 Å were used, since the phasing power falls far less than 1.0 at higher resolution. Other derivative data, both isomorphous and anomalous data of the Au-derivative and isomorphous data of the Hg-derivative, were used up to 2.6 Å resolution. The B-factors that converged to less than 5.0 $Å^2$ were fixed to 5.0 $Å^2$ and not refined further. The refined heavy atom parameters and the phasing statistics are shown in Table 3-3 and Table 3-4, respectively.

The MIR phases were improved using the solvent flattening method (Wang, 1985). The electron density map at 2.6 Å resolution calculated from the phases after solvent flattening showed some secondary structures, especially α helices. However, the electron densities of loop regions and β strands were still ambiguous. Therefore part of the polypeptide chain was traced using TURBO-FRODO. The coordinate of 3α,20β-hydroxysteroid dehydrogenase (Ghosh *et al.*, 1994), the first structure determined among the SDR family enzymes, was useful as a reference for the main-chain tracing. Then the partial model-derived phases were combined with the MIR phases using σ_A weighting, followed by refinement with solvent flattening. The improved electron density map was used for further model building. This cycle was repeated throughout the modeling process. Improvement of the mean figure of merit values during the refinement process is summarized in Table 3-5. After the TR-II subunit had been traced with a poly-alanine model, the partial model was refined with positional refinement using X-PLOR (Brünger, 1992b), after which most side chains were added to the model.

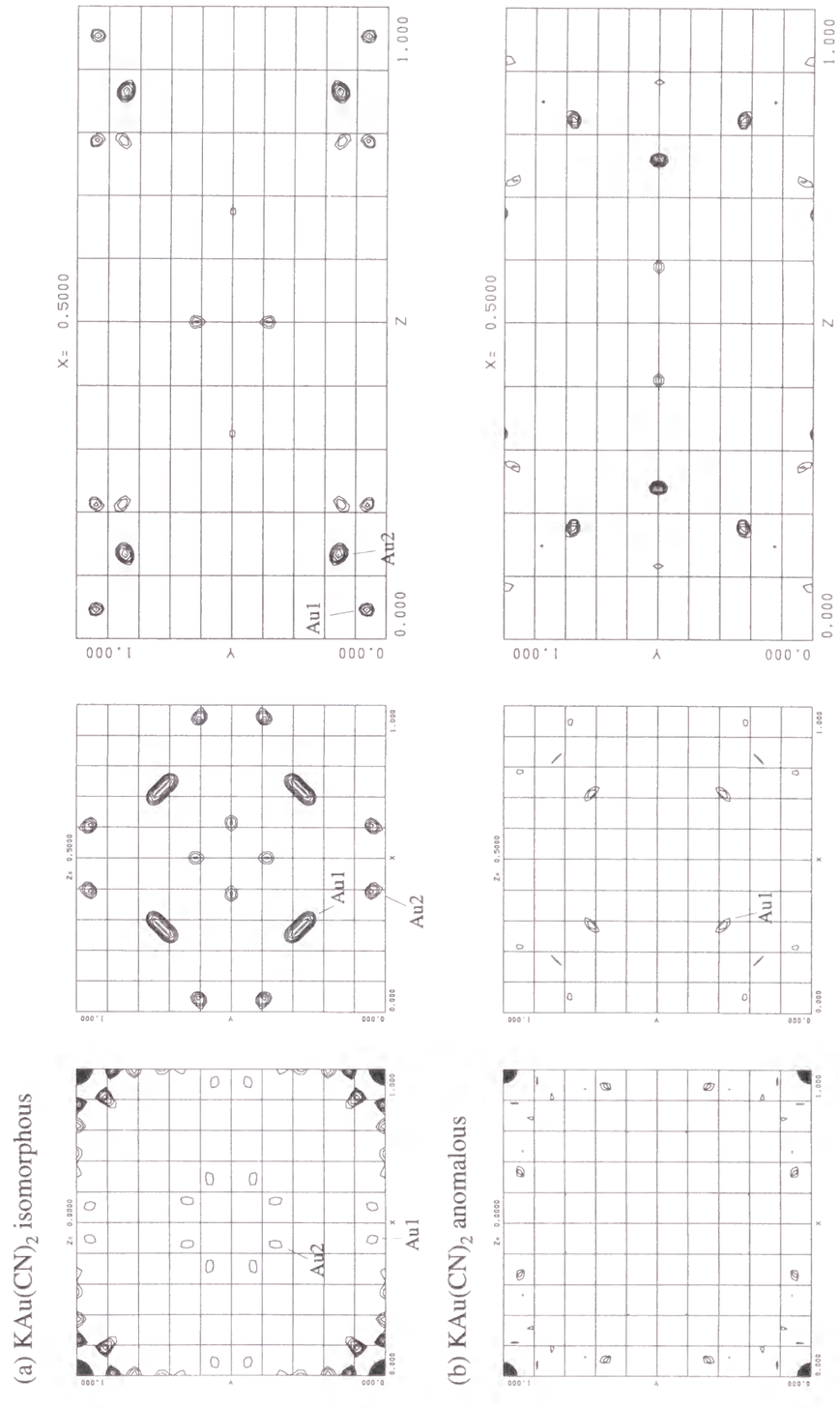

Figure 3-1. The Harker sections of difference Patterson maps calculated from the heavy atom derivative data. The Harker sections are $u = 0.5$, $v = 0.5$, $w = 0$ and 0.5. The three maps of w (Z) = 0, 0.5 and u (X) = 0.5 sections are shown for each data. Sigma cutoff is 3 sigma. (a) $KAu(CN)_2$ isomorphous difference data. (b) $KAu(CN)_2$ anomalous difference data. (c) $HgCl_2$ isomorphous difference data. (d) $HgCl_2$ anomalous difference data.

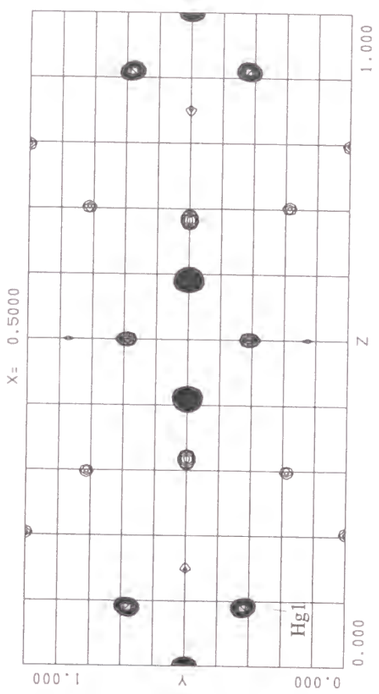

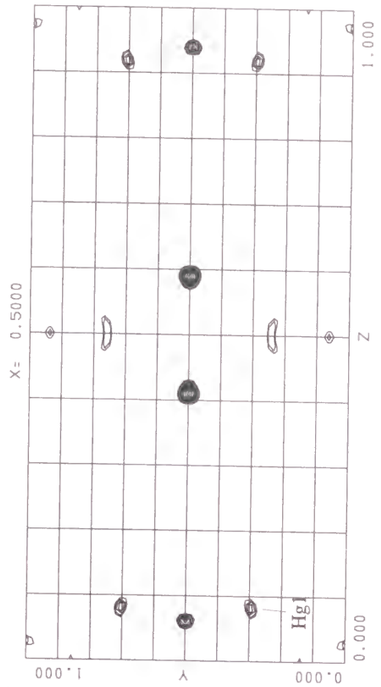

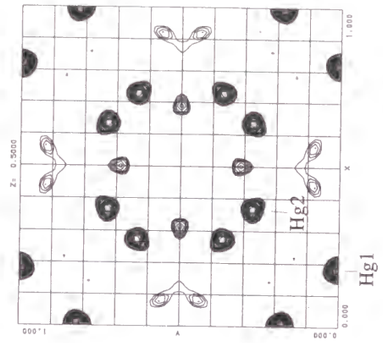

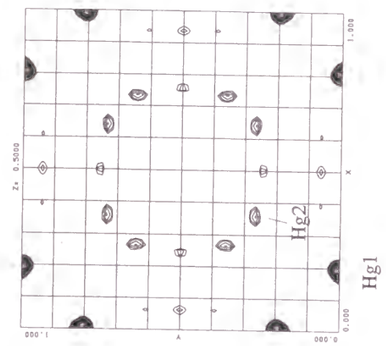

(c) $HgCl_2$ isomorphous

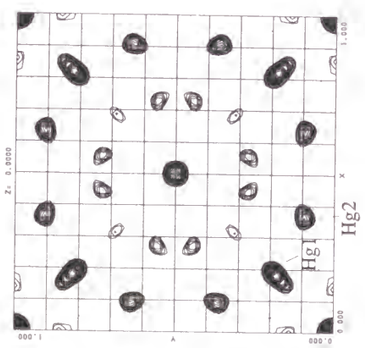

(d) $HgCl_2$ anomalous

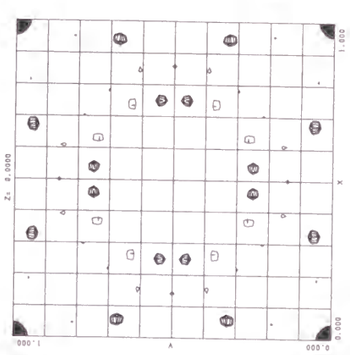

Figure 3-1. — *continued.*

Table 3-3. Refined heavy atom parameters.

Derivative	Site	x[a]	y[a]	z[a]	Occ.[b]	B[c]	Res.[d]	P.P.[e]	R_K[f]	R_C[g]
Au iso	Au1	0.219	0.024	0.727	1.00[h]	29.7	2.6	1.58	0.050	0.610
	Au2	0.721	0.166	0.860	0.80	17.5				
Au ano	Au1	0.219	0.024	0.727	1.00[h]	5.0[i]	2.6	1.35	0.110	
	Au2	0.723	0.164	0.860	0.89	5.0[i]				
Hg iso	Hg1	0.406	0.084	0.296	1.00[h]	43.6	2.6	1.48	0.040	0.575
	Hg2	0.184	0.044	0.701	0.62	32.0				
Hg ano	Hg1	0.404	0.082	0.296	1.00[h]	5.0[i]	3.0	1.19	0.050	
	Hg2	0.183	0.046	0.702	0.69	27.4				

[a]x, y, z: Fractional coordinate. [b]Occ.: Occupancy. [c]B: Temperature factor (Å^2).
[d]Res.: Resolution (Å).
[e]P.P (Phasing Power) = $\sum |F_{Hcalc}| / \sum ||F_{PHobs}|-|F_{PHcalc}||$, where F_H is the calculated structure factor amplitude of the heavy atom, and F_{PHobs} and F_{PHcalc} are the observed and calculated structure factor amplitudes of the derivative crystals, respectively.
[f]R_K (Kraut R factor) = $\sum ||F_{PHobs}| - |F_{PHcalc}|| / \sum |F_{PHobs}|$, for all acentric reflections of the isomorphous data, and
$= \sum (|F_{PH}(+)_{obs}| - |F_{PH}(-)_{calc}| + |F_{PH}(-)_{obs}| - |F_{PH}(-)_{calc}|) / \sum (|F_{PH}(+)_{obs}| - |F_{PH}(-)_{obs}|)$, for all acentric reflections of the anomalous data.
[g]R_C (Cullis R factor) = $\sum |||F_{PHobs}| \pm |F_{Pobs}|| - |F_{Hcalc}|| / \sum ||F_{PHobs}| \pm |F_{Pobs}||$, for all centric reflections.
[h]The occupancy of the major heavy atom site of each data was fixed to 1.0.
[i]These B-factors were fixed to 5.0 Å^2 during refinement.

Table 3-4. Phasing statistics.

	Resol. (Å)	P. P[a]	Mean bias[b]	No. of refl.
$KAu(CN)_2$ isomorphous	9.18	2.25	85.8	786
	5.17	1.76	89.1	786
	4.29	1.47	88.8	786
	3.80	1.18	86.2	786
	3.48	1.32	90.8	786
	3.24	1.53	90.1	786
	3.05	1.71	89.4	786
	2.90	1.70	87.5	786
	2.77	1.62	81.3	786
	2.65	1.45	86.2	786
($<m>^c$ = 0.315, M.R.E.[d] = 0.45)	∞ - 2.60	1.58	87.5	7860

Table 3-4. *—continued.*

	Resol. (Å)	P.P.[a]	Mean bias[b]	No. of refl.
$KAu(CN)_2$ anomalous	7.58	1.59	92.5	633
	4.82	1.49	92.1	633
	4.09	1.37	94.9	633
	3.68	1.38	92.0	633
	3.39	1.25	90.7	633
	3.18	1.25	95.5	633
	3.01	1.33	95.8	633
	2.87	1.32	95.0	633
	2.75	1.30	98.4	633
	2.65	1.25	101.5	633
(<*m*> = 0.244, M.R.E. = 0.50)	2.60	0.99	118.0	9
	∞ - 2.60	1.35	94.9	6339
$HgCl_2$ isomorphous	9.03	2.47	87.8	805
	5.14	2.04	88.5	805
	4.27	1.75	90.4	805
	3.78	1.45	90.4	805
	3.46	1.33	91.4	805
	3.22	1.32	88.5	805
	3.04	1.24	91.6	805
	2.89	1.07	96.2	805
	2.76	0.95	92.7	805
	2.65	0.82	104.1	805
(<*m*> = 0.299, M.R.E. = 0.46)	2.60	0.78	59.0	5
	∞ - 2.60	1.48	92.1	8055

Table 3-4. *—continued.*

	Resol. (Å)	P.P.[a]	Mean bias[b]	No. of refl.
$HgCl_2$ anomalous	8.52	1.42	86.4	418
	5.47	1.39	90.2	418
	4.66	1.40	88.1	418
	4.19	1.22	86.8	418
	3.87	1.29	87.7	418
	3.64	1.11	84.7	418
	3.45	1.10	80.6	418
	3.29	1.05	80.4	418
	3.16	1.15	79.7	418
	3.05	0.91	76.4	418
	3.00	1.33	60.4	4
(<*m*> = 0.241, M.R.E. = 0.50)	∞ - 2.60	1.19	84.1	4184

[a]Phasing power = $\sum |F_{Hcalc}| / \sum ||F_{PHobs}| \setminus |F_{PHcalc}||$

[b]Mean bias should be 90 degrees, otherwise the data set is likely to be biasing the results.

[c]<*m*> (mean figure of merit)= $|F(hkl)_{best}| / |F(hkl)|$

[d]M.R.E. (mean relative error) = $(1/N)\sum (\varepsilon(\phi)^2 / 2E^2)$, where $\varepsilon = F_{PHobs} - F_{PHcalc}$, $E = |F_{PH} \pm F_P| - F_H$, should be about 0.5.

Table 3-5. Mean figure of merit after each phase improvement steps.

Phasing and improvement step	<*m*>[a]		Phasing and improvement step	<*m*>[a]
MIR	0.558	→	Solvent flattening	0.826
↓				
Phase combination	0.694	→	Solvent flattening	0.848

[a]<*m*> (figure of merit) = |F(hkl)best| / |F(hkl)|. 8101 reflections of $F > 2\sigma(F)$ up to 2.6 Å were used for phase calculation.

The structure model containing 246 residues out of the total 259 residues was refined with the simulated annealing procedures using the slow-cool protocol (Brünger *et al*., 1990) against the 10.0 - 2.6 Å data. The *R*-factor dropped to 27.1 % (R_{free} = 39.8 %) starting from the initial value of 41.5 %. Water molecules were included when the *R*-factor dropped to about 26 %. After several cycles of model rebuilding, simulated annealing, positional refinement and overall or group B-factor refinement, the *R*-factor for 10.0 - 2.5 Å data dropped to 23.2 % (R_{free} = 35.4 %). However the electron densities for the segments of the residues from Glu8 to Cys10 and from Thr194 to Gln202 were still ambiguous and their structure models could not be built. Then the maximum likelihood residual minimization method was applied for further structure refinement using the program REFMAC (Murshudov *et al*., 1997). In the refinement process with REFMAC, σ_A, m and D were estimated from reflections not included in the refinement, so called 'free' reflections (Brünger, 1992a). Using the 'free' reflections means that this error estimate is less biased towards the existing model. As a result, obtained SIGMAA style ($2m|F_o|-|F_c|$) and ($m|F_o|-|F_c|$) maps showed the electron density for the segment of Glu8 to Cys10 and allowed successful model building of this region. In addition, these maps showed strong electron density between Cys39 and Cys65, and it was identified that these two cysteine residues made a disulfide bond in the crystal. This disulfide bond seems to be formed since DTT was removed from the native crystal. The model was further refined with gradually including higher resolution data. Although the diffraction data up to 2.0 Å was collected, the resolution range of 2.3 - 2.0 Å was not included for the refinement. This is because the completeness of this range was rather low (57 %) and if this resolution range was included, the stereochemical properties of the model became slightly worse.

The final model containing 252 amino acid residues and 103 solvent molecules was refined to the *R*-factor of 20.5 % (R_{free} = 30.6 %) for the reflections between 10.0 and 2.3 Å resolution. The refinement statistics are summarized in Table 3-6, and a Ramachandran plot is shown in Figure 3-2. Ninety percent of the total non-glycine and non-proline residues (197 residues) are observed in the most favored regions, and other residues except for Glu137 are within allowed regions. The maximum coordinate error of the TR-II structure was estimated as 0.30 Å from a Luzzati plot (Luzzati, 1952) as shown in Figure 3-3. The plot of the averaged B-factor of the main chain atoms is shown in Figure 3-4.

Table 3-6. Refinement statistics of TR-II.

Resolution range (Å)	10.0 - 2.3
No. of reflections used in refinement[a]	10999
R^b (%)	20.5
$R_{free}{}^c$ (%)	30.6
No. of atoms	
Protein	1922
Water	103
R.m.s.d from ideal value	
Bond length (Å)	0.008
Bond angle (°)	1.33
Dihedral angle (°)	23.37
Improper angle (°)	1.10
Ramachandran plot	
Most favored (%)	90.0
Additional (%)	9.6
Disallowed (%)	0.4
Average B-factor (Å^2)	
Main chain	30.17
Side chain	33.09
Solvent	36.44

[a]Reflections of $F>2\sigma(F)$ were used.
[b]$R = \sum |F_O-F_C| / \sum |F_O|$.
[c]R_{free} was calculated using 6 % data chosen randomly and omitted from the refinement.

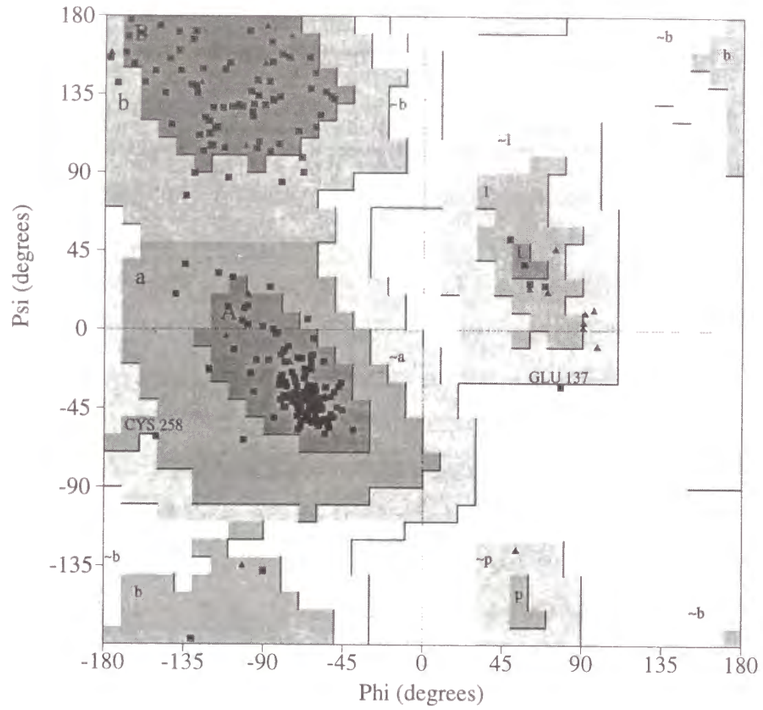

Figure 3-2. A Ramachandran plot of the crystal structure of TR-II. Triangles and squares indicate glycine and non-glycine residues, respectively. The figure was produced with PROCHECK.

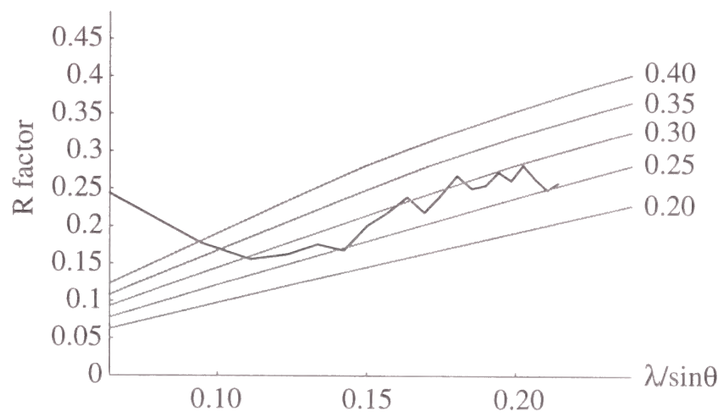

Figure 3-3. Luzzati plot for the refined crystal structure of TR-II. Gray lines are calculated Luzzati lines for coordinate errors.

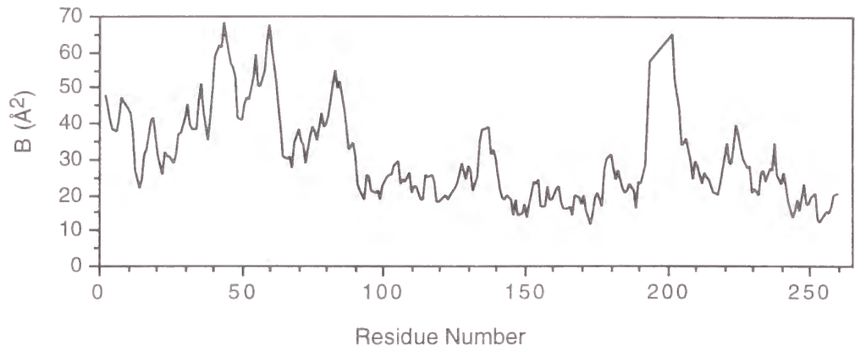

Figure 3-4. Plot of the B-factors of main-chain atoms of TR-II.

Subunit Structure

The crystal structure of TR-II is shown in Figure 3-5. The TR-II subunit comprises a single domain and is composed of seven β strands (βA - βG), creating a parallel β sheet, seven α helices (αB - αG and αG'), plus loops. Secondary structure elements are summarized in Table 3-7. The parallel β sheet is flanked on one side by three α helices αB, αC and αG and on the other by three helices αD, αE and αF. The fold represents a variant of the classic βαβ dinucleotide-binding (or Rossmann) fold widely conserved among NAD-dependent dehydrogenases (Rossmann *et al.*, 1975). In addition, αG' protrudes from this core structure. The segments prior to αG', the residues Ser195 - Ile201, could not be modeled in the protein structure because the electron density of this part was ambiguous. This result suggests that the segment is flexible and disordered in the crystal. Although addition of tropinone was necessary for the crystal growth, electron density of bound tropinone could not be found throughout the refinement process. This may be because tropinone did not bind sufficiently at the binding site in the crystal.

The ribbon diagram of a subunit of TR-II reveals the same arrangement of β-strands and α-helices in the core as has been observed in the structures of other SDR enzymes determined already (Bauer *et al.*, 1992; Varughese *et al.*, 1992; Ghosh *et al.*, 1994; Ghosh *et al.*, 1995; Rafferty *et al.*, 1995; Andersson *et al.*, 1996; Tanaka *et al.*, 1996a; Tanaka *et al.*, 1996b), even though the amino acid sequence identity is about 30 % or less among these enzymes. For instance, TR-II and *E. coli* 7α-hydroxysteroid dehydrogenase (7α-HSDH) (Tanaka *et al.*, 1996b) share only a 33 % amino acid sequence identity, but the core part of these enzymes can be superimposed with the root mean square deviation (r.m.s.d.) of 1.26 Å calculated from the

(a)

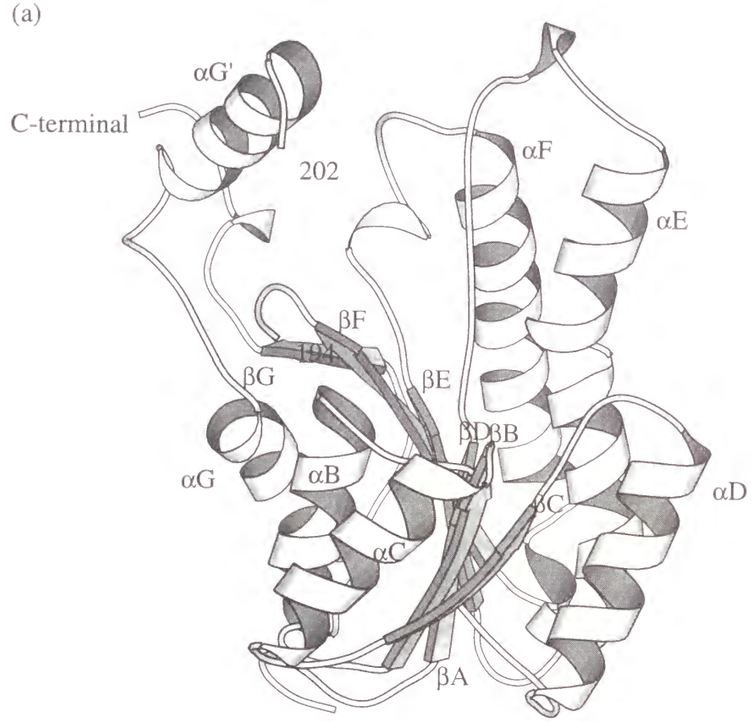

(b)

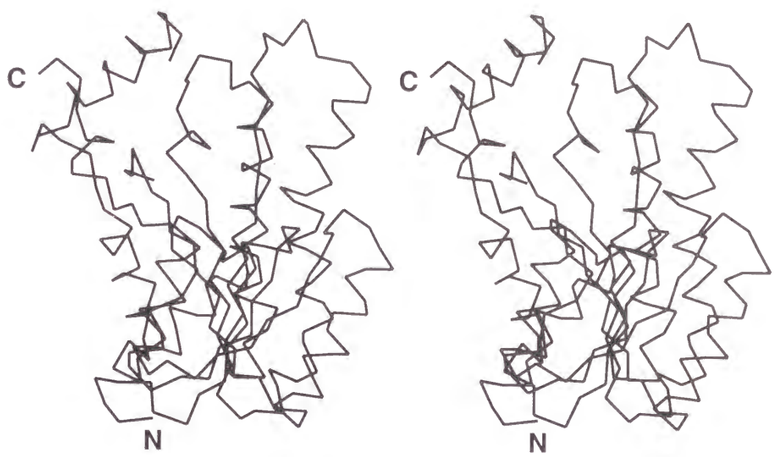

Figure 3-5. The overall fold of the TR-II subunit. (a) Ribbon diagram of the TR-II subunit. The figure was generated with the program MOLSCRIPT (Kraulis, 1991). (b) Stereo view of the Cα backbone trace of TR-II. The N and C termini are marked. The figure was generated with TURBO-FRODO. (c) Folding topology of TR-II. Helices are represented by boxes and strands by arrows. The region that structure is unknown (195 - 201) is indicated by a dashed line.

(c)

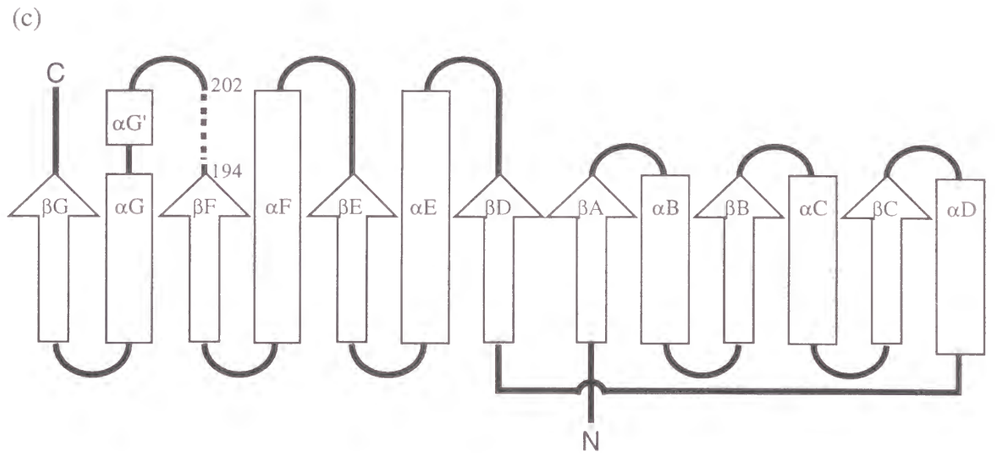

Figure 3-5. *—continued.*

Table 3-7. Secondary structures in TR-II.

α-helix	residues			β-strand	residues		
				βA	Thr11	—	Thr15
αB	Gly20	—	Ser31	βB	Ser35	—	Ser40
αC	Gln43	—	Ser55	βC	Val60	—	Val64
αD	Arg70	—	His83	βD	Ile90	—	Asn93
αE	Val108	—	Lys134	βE	Gly139	—	Ile144
αF	Ala157	—	Asp180	βF	Ile182	—	Pro189
αG'	Pro204	—	Asp215				
αG	Pro225	—	Cys236	βG	Ile247	—	Val250

214 Cα positions. On the other hand, the C-terminal regions, such the part as αG' in TR-II, exhibits greater structural variability.

Dimer Structure

In the crystal structure, TR-II subunits related by the crystallographic two-fold axis form the closest dimeric association (Figure 3-6). At the dimer interface, two long helices, αE and αF, from each subunit form a four-helix bundle. A number of hydrophobic interactions are found between these helices, and several hydrogen-bonding are found between the helix and loop region. The interactions between subunits are listed in Table 3-8. The subunit assembly of TR-II from *D. stramonium* has been unclear so far, because the results from molecular weight estimation using gel filtration were ambiguous (Nakajima *et al.*, 1994; Portsteffen *et al.*, 1994). This crystal structure indicates that TR-II is a dimer enzyme. TR-I from *D. stramonium* have also been reported as a dimer enzyme (Portsteffen *et al.*, 1994).

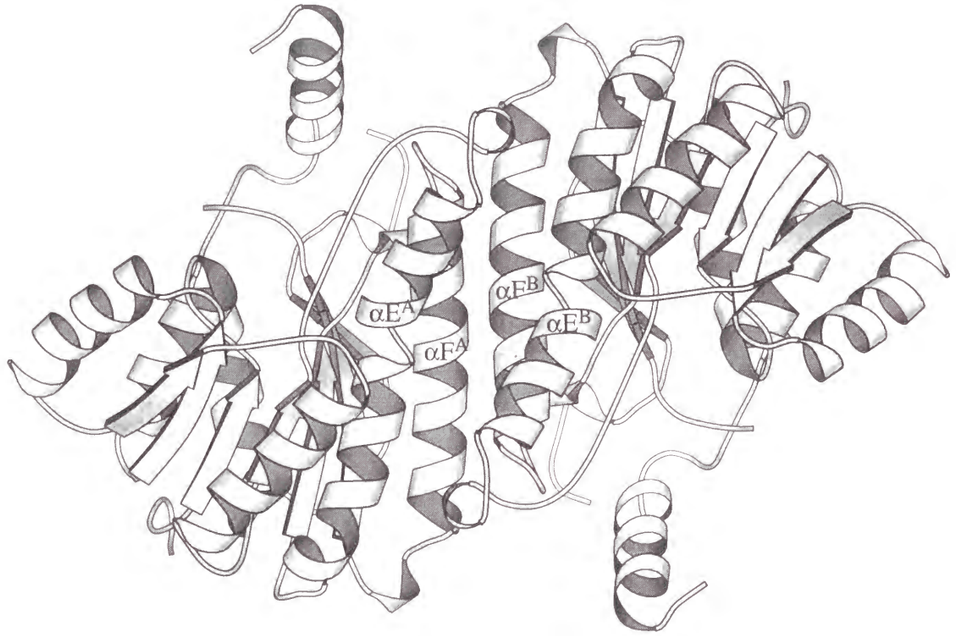

Figure 3-6. Ribbon diagram of the dimer structure of TR-II. The two subunits are related by a crystallographic two-fold axis of symmetry, perpendicular to the plane of this sheet at the center of the four-helix bundle (comprising αE^A and αF^A from the subunit A, and αE^B and αF^B from the subunit B). The figure was generated with MOLSCRIPT.

Table 3-8. Interactions between subunits.

Subunit A				Subunit B			Distance (Å)	Property
	Ala103	N	— (αF)	Glu176	OE1	2.86	H-bond
		O	— (αE)	Tyr123	OH	2.61	H-bond
		CB	— (αF)	Leu173	CD2	3.66	hydrophobic
(αE)	Tyr111	OH	— (αE)	Glu120	OE2	2.99	H-bond
		CE1	— (αE)	Phe119	CE2	3.61	hydrophobic
(αE)	Met115	CE	— (αE)	Phe119	CE2	3.53	hydrophobic
			—		CD2	3.61	hydrophobic
(αE)	Tyr123	CE2	— (αF)	Val158	CG2	3.79	hydrophobic
	Gly149	O	— (αF)	Gln168	NE2	3.13	H-bond
	Ala150	O	— (αF)	Gln168	NE2	3.27	H-bond
			— (αF)	Arg171	NE	3.42	H-bond
	Ala152	CB	— (αF)	Phe175	CD2	3.56	hydrophobic
					CE2	3.85	hydrophobic
(αF)	Ala161	CB	— (αF)	Ala165	CB	3.81	hydrophobic
(αF)	Ala165	CB	— (αF)	Ala165	CB	3.90	hydrophobic

All the SDR enzymes analyzed using X-ray crystallography so far form either a dimer or a tetramer of identical subunits. The mode of the subunit interaction observed in TR-II is common in other dimeric SDRs (Varughese *et al.*, 1992; Ghosh *et al.*, 1995), as well as in *Q*-axis related (Rossmann *et al.*, 1973) pairs of subunits of tetrameric SDRs (Ghosh *et al.*, 1994; Rafferty *et al.*, 1995; Andersson *et al.*, 1996; Tanaka *et al.*, 1996a; Tanaka *et al.*, 1996b).

3-4. Discussion

Comparison of Crystal Structures between TR-II and TR-I

For the purpose of elucidation of the stereospecific reaction mechanism of TRs, it is indispensable to compare the three-dimensional structures of TR-II and TR-I. The structure

determination of TR-I was carried out independently by Professor Yamada and his coworkers at Nara Institute of Science and Technology, Japan (Nakajima *et al.*, 1998). TR-I was crystallized as a complex with $NADP^+$, and an asymmetric unit of the crystal contains a TR-I dimer. The crystal structure of TR-I was determined with the single isomorphous replacement method with the anomalous scattering technique using an EMTS-derivative crystal. The TR-I model contains the residues 16 - 205 and 219 - 273 of one subunit (referred to as subunit A) and the residues 16 - 273 of the other (subunit B), as well as two $NADP^+$ and 98 water molecules per dimer. The *R*-factor of the model was 15.5 % (R_{free} = 24.8 %) for the reflections between 10.0 and 2.4 Å resolution.

The structure of TR-I subunit B is shown in Figure 3-7a. There is a seven-stranded parallel β-sheet flanked on each side by three α-helices in the core of TR-I, and a small lobe containing two α-helices that protrudes from the core. Structure comparison of both TRs revealed that TR-II has very similar overall structure to the TR-I structure. Conservation in the subunit structures between TR-II and TR-I is evidenced by Figure 3-7b where the two structures were superimposed by a least squares procedure using all the equivalent Cα positions. The r.m.s.d. between two superimposed structures was 0.78 Å. Furthermore, the mode of dimer formation is also identical for TR-II and TR-I; forming a four-helix bundle made up of two αE and two αF helices (Figure 3-7c). On the other hand, the corresponding region to the disordered segment (the residues 195 - 201) in TR-II was identified as an α-helical structure in TR-I subunit B (referred to as αG"). In TR-I subunit A, however, the electron density of this region (the residues 206 - 218) was also ambiguous like that in TR-II. Therefore this region is essentially flexible in both TRs.

In TR-I structure, the bound $NADP^+$ is found at the bottom of the cleft between the core and the small lobe (Figure 3-7a). The nicotinamide ring is in the *syn* conformation consistent with the observed specificity for the B-face *pro-S* hydride transfer of both TRs (Hashimoto *et al.*, 1992) and the B-face is open to the void of the cleft (Figure 3-8a). The carboxamide group of the nicotinamide ring is anchored by the main-chain nitrogen and oxygen atoms of Ile204 and the side-chain oxygen of Thr206. The 2'- and 3'-hydroxyl groups of the nicotinamide ribose are anchored with the side-chain amino group of Lys175. The 2'-phosphate group of the adenine ribose makes electrostatic interactions with both the side-chain amino group of Lys31 and the guanidino group of Arg53.

The $NADP^+$ binding site in TR-I was compared with the corresponding area in TR-II. The residues responsible for $NADP^+$ binding and their spatial organization are highly conserved between TR-I and TR-II (Figure 3-8b). This result indicates that TR-II binds the cofactor in the

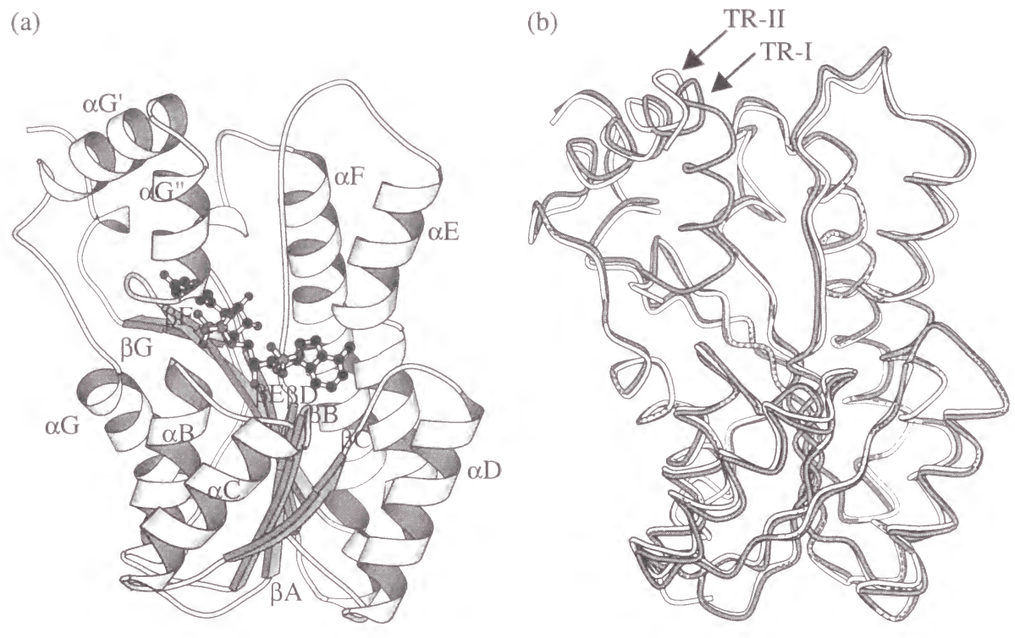

Figure 3-7. Overall structure of TR-I. (a) Ribbon diagram of TR-I subunit B. Bound $NADP^+$ is shown as a ball-and-stick model. (b) TR-II (white) and TR-I (gray) subunits are superimposed by the program LSQKAB (Collaborative Computational Project, No.4, 1994) using all the possible Cα pairs. (c) Ribbon diagram of the dimer structure of TR-I. The two subunits are related by a non-crystallographic two-fold axis, perpendicular to the plane of this sheet at the center of the four-helix bundle (comprising αE^A and αF^A from the subunit A, and αE^B and αF^B from the subunit B). The figures were generated with MOLSCRIPT.

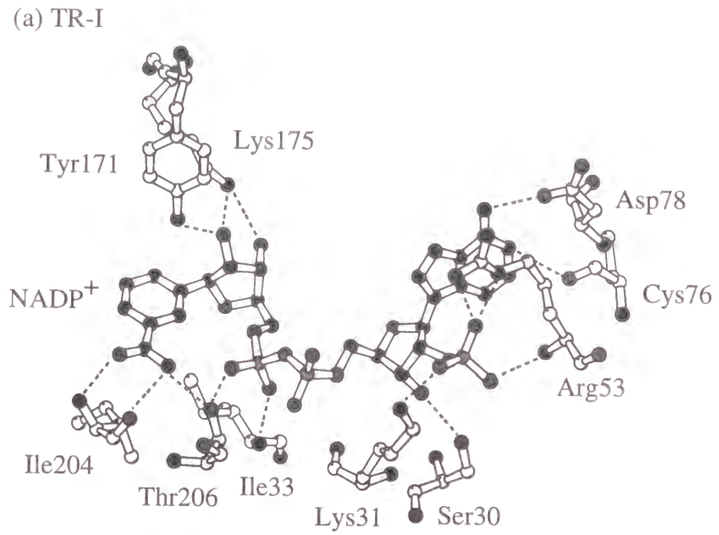

Figure 3-8. (a) $NADP^+$ binding site in TR-I. Possible hydrogen bonding interactions are indicated by dashed lines. (b) The region in TR-II corresponding to the TR-I $NADP^+$ binding site. The figures are generated with MOLSCRIPT.

same way as TR-I. There are a few residues in TR-II, such as Arg19 and Arg41, that have different side-chain conformations from the corresponding TR-I residues, Lys31 and Arg53. These differences may be caused by the cofactor binding to TR-I, since these two basic residues have been postulated to be of functional importance in binding NADPH preferably to NADH (Nakanishi *et al.*, 1996; Tanaka *et al.*, 1996a).

The catalytic mechanism of TRs has been considered from the proposed mechanism of SDRs. At present, the 'Ser-Tyr-Lys catalytic triad' is considered important in the SDR catalysis, in which the Tyr functions as an acid-base catalyst for proton transfer (Ghosh *et al.*, 1994; Ghosh *et al.*, 1995; Jörnvall *et al.*, 1995; Rafferty *et al.*, 1995; Andersson *et al.*, 1996; Azzi *et al.*, 1996; Breton *et al.*, 1996; Tanaka *et al.*, 1996a; Tanaka *et al.*, 1996b). When the subunit structures of both TRs were compared to the structure of 7α-HSDH, Ser146, Tyr159 and Lys163 in TR-II were found at the similar position of the proposed catalytic residues in 7α-HSDH, Ser146, Tyr159 and Lys163, respectively (Figure 3-9). In TR-I, the positions of the $NADP^+$ molecule as well as these catalytic residues were conserved. This structural conservation indicates that the reaction mechanism common to the SDR family also operates in both TR enzymes; tropinone is reduced by the concerted transfer of a hydride from NADPH to the C3 carbon and a proton from the Tyr residue to the carbonyl oxygen.

Implication for Stereospecificity of TRs

Structure comparison between two TRs has indicated that both TRs have the common overall structure, cofactor-binding mode and catalytic mechanism. Therefore, in order to achieve the differentiation of stereospecificity, TR-II and TR-I seem to bind their substrate in different manner.

Tropinone-binding in TRs was presumed on the basis of the product configuration and the stereochemical arrangement toward the *pro-S* hydride of the bound cofactor and the catalytic Tyr residue; tropinone should bind at the same site, the cleft between the core and the small lobe in TR-II and TR-I, but in opposite orientations. That is, tropinone binds to TR-II facing its α side (the opposite side of the seven-membered ring from the methylamine side) toward *pro-S* hydrogen of NADPH, whereas it binds to TR-I facing its β side (the same side of the seven-membered ring as the methylamine side) (Figure 3-10). The structures of predicted tropinone-binding sites in TR-II and TR-I are shown in Figure 3-11, with modeled tropinone molecules. The residues around the predicted tropinone molecules are located at the two loops and αF in the core, and at the small lobe. Most of the residues in this area are hydrophobic, and these residues could provide an environment favorable for binding tropinone that generally has

Figure 3-9. The positions of the conserved catalytic residues (Ser, Tyr, Lys). These residues, NADP+ and a substrate (7-oxoglycochenodeoxycholic acid (GCDCA) in 7α-HSDH) are shown as ball-and-stick models. (a) TR-II. (b) TR-I. The bound NADP+ is also shown. (c) 7α-HSDH. The bound NADH and GCDCA are also shown. The coordinate 1FMC in Brookhaven Protein Data Bank was used. The figures are generated with MOLSCRIPT.

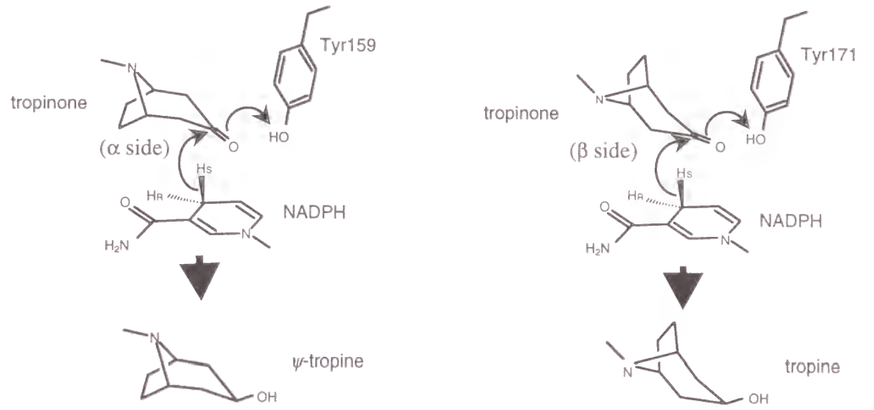

Figure 3-10. Predicted binding orientation of tropinone toward $NADP^+$ and the catalytic residue.

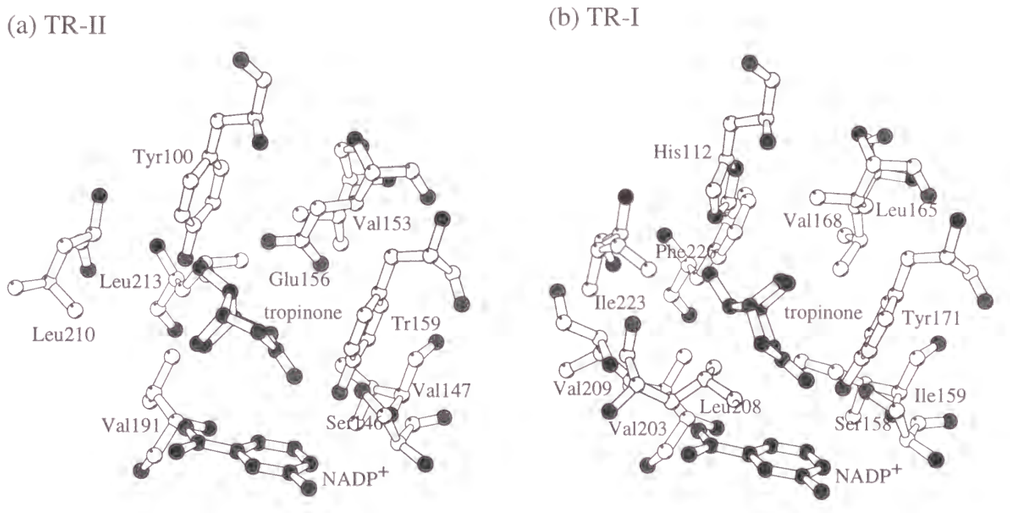

Figure 3-11. Prediction of the tropinone binding sites in TRs. Modeled substrates are also shown. (a) TR-II. (b) TR-I. The figures are generated with MOLSCRIPT.

a hydrophobic nature. However, there are several charged residues in the binding site. In TR-II, Glu156 is located near the amine group of the predicted tropinone molecule, which is replaced by the hydrophobic Val168 in TR-I. On the other hand, in TR-I there is a basic residue His112, which in TR-II is replaced by Tyr100, a polar but not basic residue. As the nitrogen atom of tropinone is positively charged under physiological pH conditions (Portsteffen *et al*., 1994), location of these charged residues in the tropinone-binding sites agreed well with the predicted orientations of tropinone. In TR-II, attraction between positive charge of the amine moiety of substrates and negative charge of Glu156 may fix the binding orientation of the substrates properly. On the other hand, if the substrate in TR-I binds in the same orientation as in TR-II, the positive charge of His112 may cause charge repulsion with the substrate. In order to avoid this repulsion, TR-I enzymes may adopt the "upside-down" binding orientation of the substrate.

The mechanism to maintain the opposite stereospecificities of TRs is consistent with the results of the several biochemical experiments reported so far. For example, TR-II has relatively high affinity for tropinone than TR-I (Hashimoto *et al*., 1992; Nakajima *et al*., 1994; Portsteffen *et al*., 1994). This seems to be because the polar amine moiety of tropinone can interact electrostatically with Glu in TR-II, on the other hand it has to face to the hydrophobic surface of the binding site in TR-I. This implication is also supported by the report that the K_m value for tropinone in TR-I is decreased by increasing the reaction pH (Portsteffen *et al*., 1994). This result indicated that elimination of the positive charge from tropinone improves its affinity for TR-I. The same report also showed that 8-thiabicyclo[3,2,1]octane-3-one (Figure 3-12), a non-charged analog of tropinone, could not be reduced by TR-II but could be reduced to either of the two possible stereoisomers by TR-I. This result also supported that the charge on the nitrogen atom of tropinone is crucial for the binding in TR-II and for the strict stereospecificity in TR-I.

These TR-II and TR-I structures are the first determined structures of a pair of enzymes that have high sequence similarity but have opposite reaction stereospecificity. The enzymes for which structural analyses from the view point of stereospecificity were performed so far are

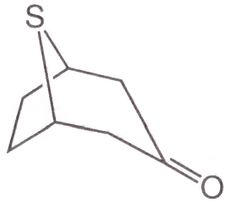

Figure 3-12. Chemical structure of 8-thiabicyclo[3,2,1]octane-3-one.

evolutionally very distant. For example, D-LDH and D-amino acid aminotransferase (D-AAT) have completely different overall structures from those of respective enzymes with normal stereospecificity (L-LDH and L-AAT) (Sugio *et al*., 1995; Stoll *et al*., 1996). Therefore both pairs of enzymes prepare their active sites by structure convergence to provide same catalytic functions. In contrast, the results from the comparison of the two TR structures suggest that opposite reaction stereospecificity can be accomplished by changing several residues in the active site with a conserved protein framework.

CHAPTER 4

Crystal Structure of Tropinone Reductase-II Complexed with $NADP^+$ and Pseudotropine

4-1. Introduction

In the preceding chapter, it was presumed that the reaction stereospecificity is controlled by several residues such as Glu156 in TR-II and His112 in TR-I. However, in order to elucidate enzyme-substrate interactions at the active site and to propose a putative mechanism description in more detail, it is necessary to analyze a high-resolution structure of the enzyme complexed with the substrate and the cofactor. Therefore a high-resolution structural analysis of a TR-II ternary complex with the cofactor and the substrate has been undertaken.

Complexes of macromolecules can be obtained either by soaking pre-formed crystals in a ligand solution, or by cocrystallizing directly from protein solution which is previously complexed with ligands. Soaking of crystals whose structure has been determined in that crystal form reduces the complexity of the crystallographic problem to that of determining the positions of the newly introduced atoms using difference Fourier methods. However, in some cases ligands cannot be introduced to the binding sites sufficiently because of the restrictive effects of lattice contacts. On the other hand, cocrytallization can avoid such restrictive effects, but the obtained crystals may be non-isomorphous to the crystals of the unliganded enzymes. In this case the molecular replacement (MR) method is necessary for the structure determination.

The MR method is a way to transfer the known protein molecular structure from its crystalline arrangement to the crystal of the protein for which the structure is not yet known (Rossmann and Blow, 1962). Placement of the molecule in the target unit cell requires its proper orientation and precise position. In short, it involves two steps: rotation and translation. In the rotation step a rotation matrix is searched to orient the known and unknown molecules with respect to each other. In the next step a translation vector is searched to superimpose the now correctly oriented molecule onto the other molecule.

This chapter describes the crystal structure of TR-II complexed with $NADP^+$ and ψ-tropine at 1.9 Å resolution determined using the MR method. The structure of the TR-II ternary complex has revealed the substrate and the cofactor binding mode in the enzyme. The structure

of the segment which is disordered in the unliganded TR-II (CHAPTER 3) but constitutes the active site has also been elucidated. The active site structure has provided an insight to understand the architecture for its stereospecific oxidoreduction.

4-2. Experimental Procedures

Materials and Methods

Tropinone was purchased from Aldrich (Milwaukee, USA). β-NADPH and β-$NADP^+$ were purchased from Oriental Yeast Co., Ltd. (Tokyo, Japan). ^{1}H NMR spectrum was measured on a Varian VXR-200 spectrometer (200 MHz). Elemental analysis was performed on a Yanaco MT-5. Melting point was measured on a Mettler FP62 and was corrected. All reagents were purchased at highest commercial quality and used without further purification.

Synthesis of Ψ-Tropine

ψ-Tropine was prepared according to the method of Nickson and Fieser (1952). Tropinone (2.5 g, 18.0 mmol) was dissolved in a mixture of 5 ml of dry toluene and 2.06 ml of isobutanol (1.65 g, 22.3 mmol) in a dropping funnel mounted on a flask. The flask was charged with 5 ml of dry toluene and sodium (0.94 g, 40.9 mmol) and heated to boiling. Vigorous stirring was then maintained while the contents of the funnel were gradually introduced over a period of 15 minutes. More toluene (5 ml) was then added through the funnel and the mixture was vigorously stirred and kept at a gentle reflux for 2 more hours. After cooling the flask in an ice-bath, 10 ml of water was slowly added to quench the reaction mixture and stirring was maintained for an additional 10 minutes. The solution was transferred to a separatory funnel, from which the toluene layer was separated and the aqueous layer was extracted with dichloromethane. The combined extracts were evaporated and the residual oil was dissolved in hot benzene. Hexane was added to the solution, which on standing deposited colorless needles (1.06 g, 42 %). The purity of the synthetic ψ-tropine was checked by gas-liquid chromatography (Hashimoto *et al.*, 1992), and the product was found to be a single isomer: m.p. 105.8 - 107.9 °C [lit. (Nickson and Fieser, 1952), m.p. 106-108 °C]; ^{1}H-NMR ($CDCl_3$) δ 1.50-1.70 (m, 4H, 6-H and 7-H), 1.83 (ddd, J = 13.0, 6.1 and 3.0 Hz, 2H, 2-H and 4-H), 1.90-2.10 (m, 3H, 2-H, 4-H and OH), 2.31 (s, 3H, NCH_3), 3.16-3.20 (m, 2H, 1-H and 5-H), 3.89 (tt, J = 10.9 and 6.1 Hz, 1H, 3-H); Anal. Calcd. for $C_8H_{15}NO \cdot 7/100H_2O$: C, 67.46; H, 10.71; N, 9.83. Found: C, 67.45; H, 10.61; N, 9.84.

Crystallization of a TR-II Ternary Complex

Crystals of the TR-II ternary complex were obtained by cocrystallization with ligands using the hanging-drop vapor diffusion method. Crystals were grown in a 24 well Cell Culture Cluster (Costar, Cambridge, USA). Two microliters of the protein solution (15 mg/ml TR-II, 3.3 mM $NADP^+$, 16.7 mM ψ-tropine, 5 mM Tris-HCl pH 7.5 and 1 mM DTT) were mixed with 2 μl of the reservoir solution (0.1 M HEPES pH 7.5, 1.7 M Li_2SO_4 and 1 mM DTT) to form a hanging drop, and the drop was equilibrated over 1 ml of the reservoir solution at 20 °C. Single crystals (approximately 0.8 × 0.4 × 0.4 mm) were harvested after 2 weeks. These crystals have a space group of $P6_122$ or $P6_522$ and unit cell dimensions of $a = b = 88.59$ Å and $c = 338.34$ Å (Table 4-1).

X-ray Data Collection and Processing

X-ray diffraction data of the TR-II complex crystals were collected on the ID14/EH3 beamline at the European Synchrotron Radiation Facility (ESRF, Grenoble, France) at room temperature with a wavelength of 0.918 Å using 40 × 80 cm Fuji imaging plate detector. The crystal to film distance was 360 mm and the detector θ angle was 0 °. The oscillation angle was 3° and the exposure time was 60 s (2 passes of 30 second exposure). The data were processed with

Table 4-1. Data Collection and Processing statistics

Space group	$P6_122$
Cell dimensions (Å)	$a = b = 88.59$ $c = 338.34$
subunit / asymmetric unit	2
V_m (Å^3/Da)	3.39
V_{solv} (%)	63.7
Resolution (Å)	1.9
Observed reflections ($I > \sigma(I)$)	195899
Unique reflections ($I > \sigma(I)$)	54120
Completeness (%, overall/last shell)	85.6/77.9 (1.93-1.90 Å)
R_{merge}[a] (%, overall/last shell)	8.4/24.7

[a] $R_{merge} = |I - \langle I \rangle| / I$

DENZO and SCALEPACK (Otwinowski, 1993). Partial reflections were not included. The final data set was put on a quasi-absolute scale using TRUNCATE of the CCP4 package (Collaborative Computational Project, No.4, 1994). Data collection and processing statistics are presented in Table 4-1.

Structure Determination and Refinement

The structure of the TR-II complex was solved using the MR method with the AMORE program (Navaza, 1994) using the 'auto-amore' procedure. The single subunit structure of TR-II determined using the MIR in CHAPTER 3, omitting all solvent molecules, was used as a search model. Cross-rotation functions and translation functions were calculated using the data in the resolution range 10 - 3.5 Å. The derived models were also refined as rigid bodies with the AMORE using the data in the resolution range 10 - 3.5 Å. Further structure refinement was carried out using X-PLOR version 3.851 (Brünger, 1992b) and model rebuilding was carried out using the TURBO-FRODO program (Bio-Graphics). In subsequent positional refinement and group B factor refinement, $NADP^+$ and ψ-tropine models were included to fit Fourier maps. The parameter file and topology file for $NADP^+$ was generated with the program XPLO2D (Kletwegt and Jones, 1997) using topology.nad and param.nad (the topology and parameter file for NAD^+) in the X-PLOR package as references. The coordinates, parameter file and topology file for ψ-tropine were generated using the programs QUANTA and CHARMm (Molecular Simulations Inc.). The model was then subjected to several cycles of positional refinement, individual B factor refinement and rebuilding against data in the resolution range 10-1.9 Å. Water molecules were included using the WATERHUNTER program (Sugio *et al.*, 1995). The geometry of the model was monitored throughout the refinement using X-PLOR and PROCHECK (Laskowski *et al.*, 1993). Statistics on the refinement and the model geometry are presented in Table 4-3.

Measurement of the NADPH Content in Reaction Mixtures

The amount of NADPH in reaction mixtures of TR-II was measured spectrophotometrically. Reaction mixtures A (0.1 M HEPES pH 7.5, 1.7 M Li_2SO_4, 1 mM DTT, 3.3 mM $NADP^+$, 16.7 mM ψ-tropine and 1.0 or 5.0 μM TR-II) and B (0.1 M HEPES pH 7.5, 1.7 M Li_2SO_4, 1 mM DTT, 3.3 mM NADPH, 16.7 mM tropinone and 1.0 or 5.0 μM TR-II) were allowed to reach an equilibrium state at 20 ˚C for several days. The NADPH concentration of each solution was calculated from the absorbance at 340 nm using a molar absorption coefficient of 6200 $M^{-1}cm^{-1}$.

4-3. Results and Discussion

Structure Determination

The complex crystals were prepared by cocrystallization with $NADP^+$ and ψ-tropine, which are participants of the reverse reaction in the metabolic pathway. This is because the rate of the reverse reaction of TR-II is much slower than that of the forward reaction (Hashimoto *et al.*, 1992) and it could be expected to make a stable ternary complex with such ligands. The TR-II ternary complex was crystallized under the completely different condition from the unliganded TR-II, and obtained crystals had a different space group and cell parameters (Figure 4-1a, Table 4-1). Although the unit cell dimensions were large and the solvent content of the crystals was rather high, the crystals diffracted well to a high resolution on the third station of beamline ID14 at the ESRF, and the diffraction data allowed an analysis of the at 1.9 Å resolution.

The ternary complex structure was determined using the MR. The cross-rotation function using data in the resolution range 10 - 3.5 Å yielded two best solutions (Table 4-2). This result is consistent with the expectation of two subunits per an asymmetric unit based on the unit cell dimensions. In following a translational search using data in the resolution range 10 - 3.5 Å, both enantiomeric space groups $P6_122$ and $P6_522$ were tried, and clear solutions for both rotation functions mentioned above were detected in space group $P6_122$ (Table 4-2). One of the solutions was fixed, and the search for the other translational solution was repeated. The derived models were refined as two rigid bodies using the AMORE program, and the solution had a correlation coefficient of 0.734 and an R factor of 31.9 % for the range of 10 Å to 3.5 Å.

(a) (b)

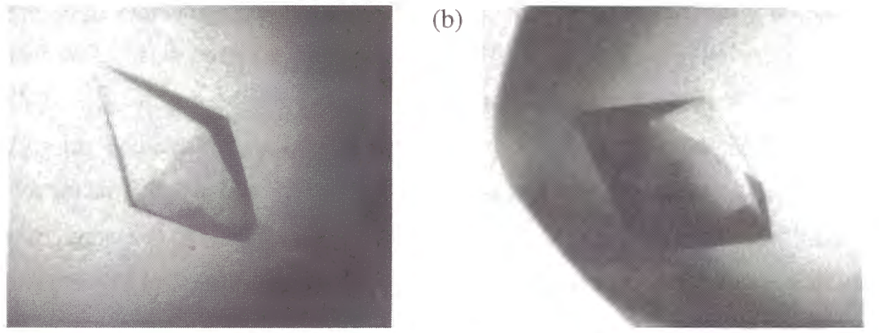

Figure 4-1. Crystals of TR-II ternary complexes. (a) A crystal grown from Li_2SO_4. This crystal form was used for structure determination. (b) A crystal grown from PEGMME550.

Table 4-2. Solutions of molecular replacement[a].

Rotation Search	Euler angles from TABFUN[b]			Euler angles from original[c]			Corr. F.[d]	Highest false[e]
	α (°)	β (°)	γ (°)	α (°)	β (°)	γ (°)		
Solution 1	15.19	77.65	98.43	135.03	-62.29	-60.82	9.1	6.6
Solution 2	50.72	62.96	237.46	134.26	61.75	-179.28	6.9	

Translation Search	Fractional coordinates from TABFUN[b]			Fractional coordinates from original[c]			Corr. F.[d]	Highest false[e]
	x	y	z	x	y	z		
Solution 1	0.255	0.276	0.434	0.177	1.348	0.070	31.8	18.4
Solution 2	0.388	0.930	0.189	-0.144	-0.970	0.264	30.5	

[a]The solutions are that was found after rigid body refinement in AMORE.
[b]Functions for the coordinate translated by tabling function in TABFUN (AMORE).
[c]Functions for the coordinate of the original model determined by MIR (CHAPTER 3).
[d]Correlation coefficients. [e]Correlation coefficient for the highest false solution.
*Solution 1 and 2 were used for conversion to the models of subunit A and subunit B, respectively.

The second solution was translated by the SYMMETRY option in the TURBO-FRODO program so that two molecules had a common origin. These two molecules are related by the spherical polar angles $\omega = 152.0$ °, $\phi = 59.9$ °, $\chi = 179.9$ °.

The electron density map calculated using the MR solutions showed clear electron densities not only for the bound $NADP^+$ and ψ-tropine but for the residues from 195 to 201, which do not exist in the unliganded TR-II coordinate. The model of the residues from 195 to 201 was built to fit Fourier maps. Refinement was then carried out using X-PLOR 3.851 (Brünger, 1992b). Non-crystallographic symmetry was not restrained throughout the refinement process. After one round of positional refinement and group B factor refinement, R-factor for 10.0 - 2.0 Å data dropped to 25.6 % (R_{free} = 28.8 %). At this stage $NADP^+$ and ψ-tropine models were included to fit Fourier maps. The model was then subjected to several cycles of positional refinement, individual B factor refinement and rebuilding against data in the resolution range 10-1.9 Å. Water molecules were included when R-factor dropped to about 21 %. The disulfide bond between Cys39 and Cys65, which was found in the unliganded TR-II

structure (CHAPTER 3), was not observed in this complex structure. This seems to be because DTT was present in the complex crystal.

The final model of the TR-II:$NADP^+$:ψ-tropine complex was a dimer including all residues except for the first residues of each subunit, which was deleted when purified from *E. coli* (CHAPTER 3). The model was refined to an R-factor of 17.2 % and R_{free} of 20.6 % for reflections between 10.0 and 1.9 Å resolution. The refinement statistics are summarized in Table 4-3. The model has 91 % of the residues in the most favored Ramachandran regions with

Table 4-3. Refinement statistics of TR-II: $NADP^+$:ψ-tropine complex.

Resolution[a] (Å)	10.0-1.90
Protein atoms	3950
Ligand atoms	116
Water molecules	236
R_{factor}[b]/R_{free} (%)	17.2/20.6
Rms deviations	
Bond length (Å)	0.007
Bond angles (deg)	1.275
Dihedral angles (deg)	23.836
Improper angles (deg)	0.806
Ramachandran plot	
Most favored (%)	90.6
Additional (%)	9.4
Disallowed (%)	0.0
Average B (Å^2)	
Main chain	16.0
Side chain	20.7
Solvent	32.3

[a]Reflections of $F > 2\sigma(F)$ were used.
[b]$R_{factor} = \sum||F_{obs}| - |F_{calc}|| / \sum|F_{obs}|$, (5 % randomly omitted reflections were used for R_{free}).

no residues in disallowed regions (Figure 4-2). The maximum coordinate error of the TR-II ternary complex structure was estimated as 0.25 Å from a Luzzati plot (Luzzati, 1952) as shown in Figure 4-3. The plots of the averaged temperature factor of the main chain atoms and the side chain atoms are shown in Figure 4-4.

At first it was attempted to prepare TR-II ternary complex crystals by soaking the native crystals with the substrate. However, these crystals did not result in clear electron densities for the substrate and the cofactor (data not shown). During the screening of the cocrystallization conditions for a TR-II ternary complex, another condition was found in which precipitants were PEG monomethyl ether 550 and $CaCl_2$ and the space group was $P6_222$ with unit cell dimensions, $a = b = 131.87$ Å, $c = 102.88$ Å (Figure 4-1b). In addition, another crystal which is the same form as the analyzed crystal was also obtained complexing with $NADP^+$ and tropinone (a non-productive complex). However these crystals also did not show clear electron density for the substrates. The crystals mentioned above were not used in further structural analysis.

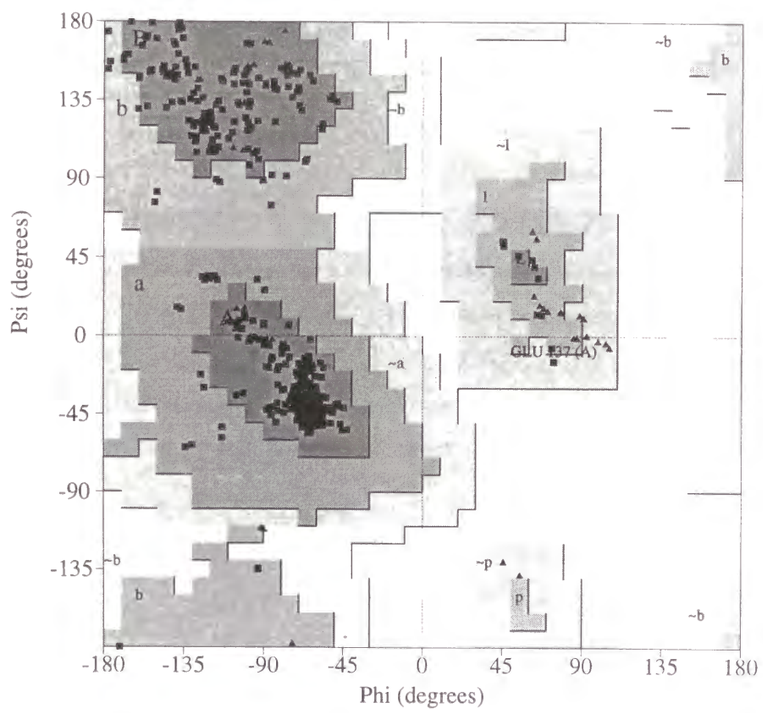

Figure 4-2. A Ramachandran plot of the crystal structure of TR-II:$NADP^+$:ψ-tropine complex. Triangles and squares indicate glycine and non-glycine residues, respectively. The figure was produced with PROCHECK.

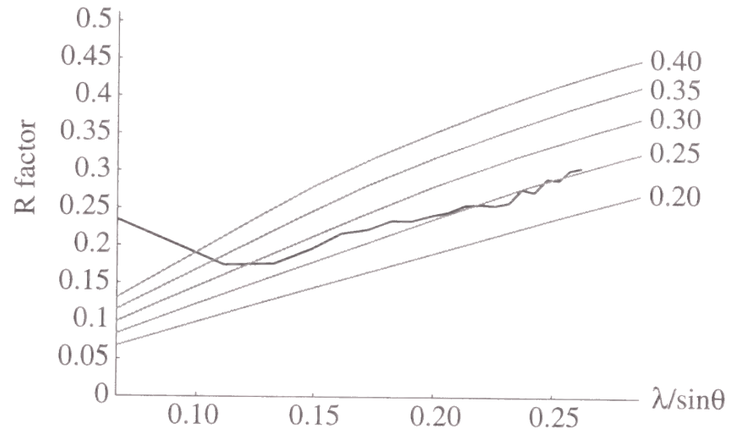

Figure 4-3. Luzzati Plot for the refined structure of the ternary complex of TR-II with $NADP^+$ and ψ-tropine. Gray lines are calculated Luzzati lines for coordinate errors.

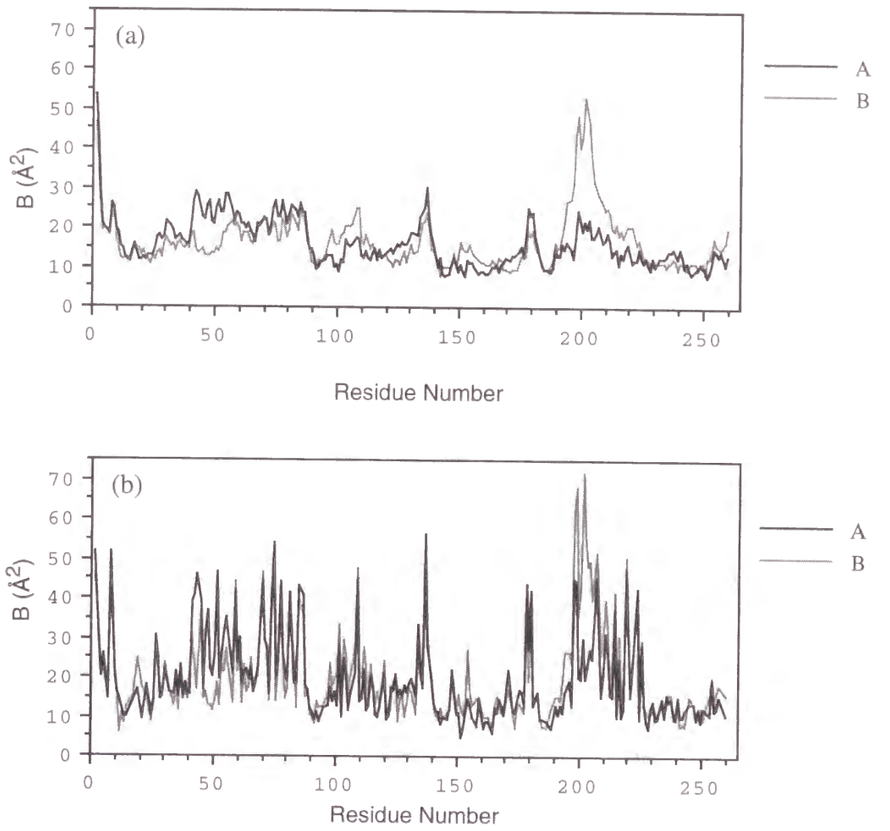

Figure 4-4. Plots of the B-factor of the TR-II:$NADP^+$:ψ-tropine complex. Black lines indicate subunit A, and gray lines indicate subunit B. (a) Main chain. (b) Side chain.

Description of the Structure

The crystal structure of the TR-II:$NADP^+$:ψ-tropine complex is shown in Figure 4-5a. A TR-II dimer in an asymmetric unit is very symmetrical and the Cα coordinates of the two subunits (subunits A and B) are superimposed with a root mean square deviation (r.m.s.d.) of 0.14 Å. The structure of subunit A is considered representative of the two subunit hereafter. The subunit structure of the ternary complex is shown in Figure 4-5b; it is an α/β doubly wound protein with the Rossmann-fold for NADPH binding. Overall, the ternary complex is similar in structure to the unliganded TR-II (CHAPTER 3), and has essentially the same secondary structure assignments. A superimposition of the subunit of the ternary complex and the unliganded structure using 252 out of 259 residues showed r.m.s.d. between Cα atoms of only 0.41 Å. Distances between Cα atoms of each structure after superimposition are plotted as Figure 4-6. The mode of the subunit interaction observed in the ternary complex was also similar to that of the unliganded structure (Table 4-4), although the distances between each residues slightly changed.

This ternary complex , however, revealed the structure of the segment between residues 195 and 201. These residues, which are disordered and not modeled in the unliganded TR-II structure, were clearly visible in the electron density map of the complex and were modeled as an α helical structure (Figure 4-5b). The corresponding part in the TR-I structure is also a helix, αG" (Nakajima *et al.*, 1998). Thus we define this segment as αG". This helix is connected to βF (N-terminal side) and αG' (C-terminal side) with two loop regions, Gly190 - Thr194 and Ile201 - Asp203, respectively. The length of αG" is 3 residues shorter than TR-I, and the C-terminal side loop is longer instead.

$NADP^+$ Binding Site

The electron density corresponding to $NADP^+$ and ψ-tropine was well defined (Figure 4-7a). The $NADP^+$ molecule binds at the bottom of the cleft between the small lobe (αG" and αG') and the core structure (the remaining main part with the Rossmann-fold). The $NADP^+$ is found in an extended conformation. The nicotinamide ring is in the *syn* conformation and has its B face oriented towards the ψ-tropine, consistent with the *pro-S* hydride transfer. Both ribose rings have the *C2'-endo* puckering.

Figure 4-8a shows the environment of the $NADP^+$ binding site. The nicotinamide ring and the pyrophosphate moiety make polar interactions with the main chain of Ile194, and the side chains of Thr194 and Ser195. These residues are located at the N-terminal side loop or the N-terminal part of αG". These interactions may hold the loop structure, therefore the position

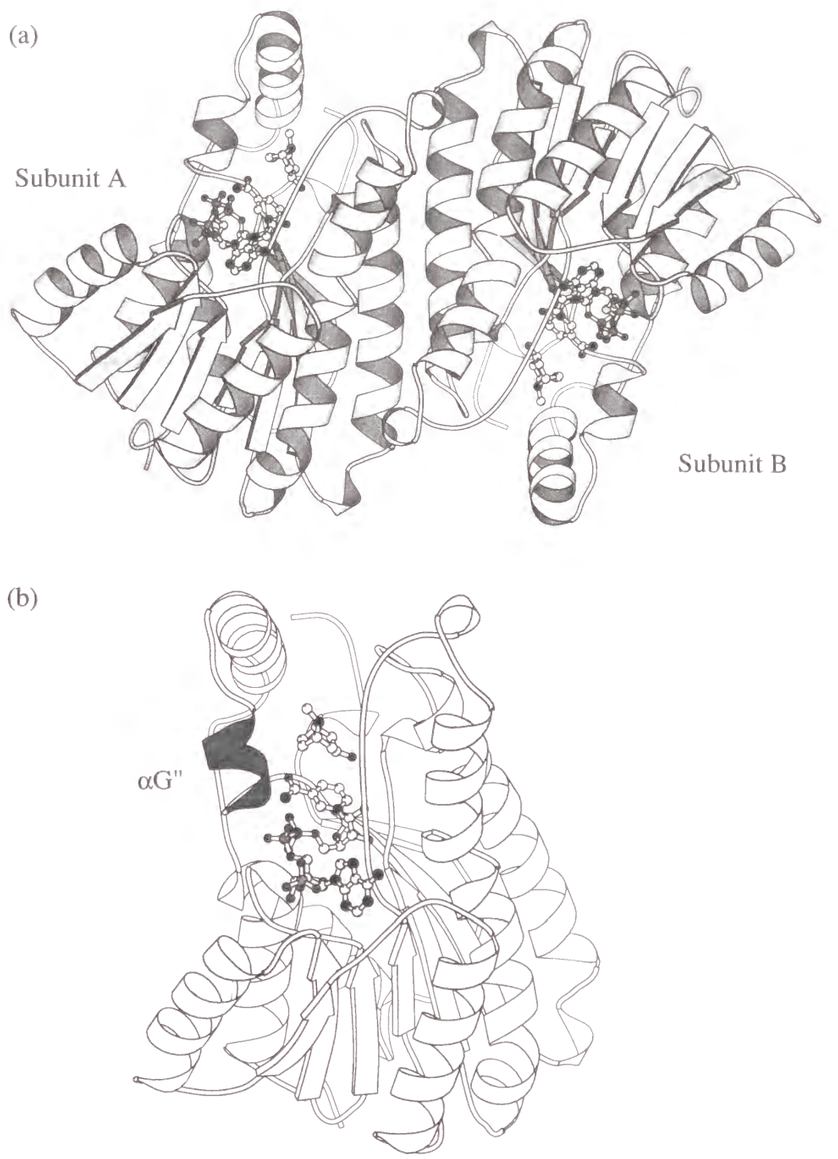

Figure 4-5. (a) Ribbon diagram of the structure of TR-II:$NADP^+$:ψ-tropine complex. Bound $NADP^+$ and ψ-tropine are shown as ball-and-stick models. The two subunits are related by a non-crystallographic two-fold axis of symmetry, perpendicular to the plane of this sheet at the center of the four-helix bundle (comprising αE and αF from each subunit). (b) Ribbon drawing of a monomeric structure of the TR-II ternary complex. Bound $NADP^+$ and ψ-tropine are illustrated in ball-and-stick models. The segment between residues 195 and 201 (αG") is shown in gray. The figures were generated with MOLSCRIPT.

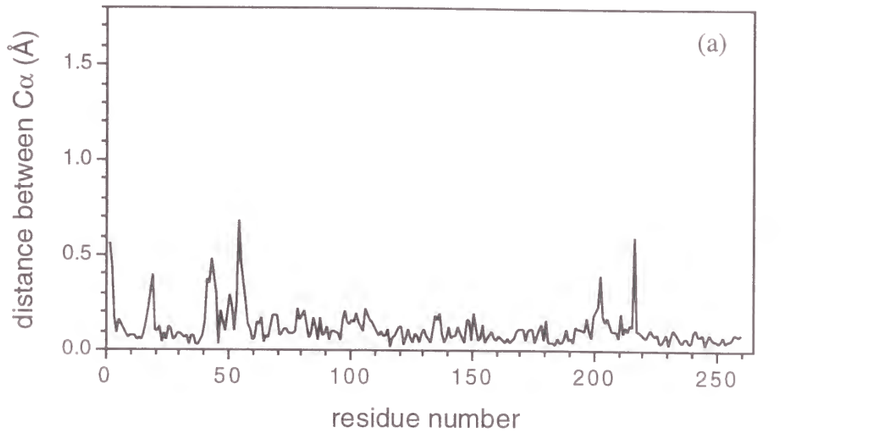

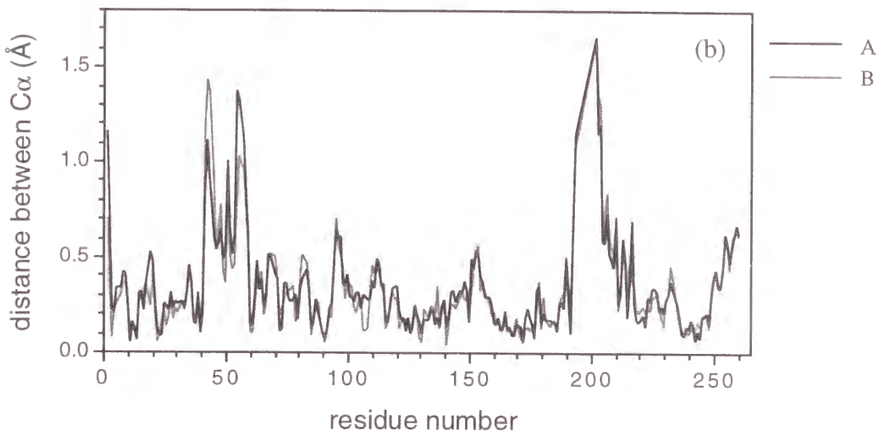

Figure 4-6. Distances between Cα atoms of each structure after superimposition with LSQKAB. (a) Distances between the TR-II ternary complex subunit A and subunit B. (b) Distances between the TR-II unliganded structure and the ternary TR-II complex. The black line indicates the distance between the unliganded TR-II and subunit A of the complex, and the gray line indicates the distance between the unliganded structure and subunit B of the complex.

Table 4-4. Interactions between subunits of TR-II:NADP$^+$:ψ-tropine compex.

Subunit A				Subunit B			Distance (Å)	Property
	Ala103	N	— (αF)	Glu176	OE2	2.96	H-bond
		O	— (αE)	Tyr123	OH	2.57	H-bond
		CB	— (αF)	Leu173	CD2	3.73	hydrophobic
(αE)	Tyr111	OH	— (αE)	Glu120	OE2	3.31	H-bond
		CD2	(αE)	Tyr123	CE2	3.91	hydrophobic
		CE1	— (αE)	Phe119	CE2	3.83	hydrophobic
(αE)	Met115	CE	— (αE)	Phe119	CE2	3.53	hydrophobic
			—		CD2	3.61	hydrophobic
(αE)	Phe119	CE2	— (αE)	Tyr111	CE2	3.93	hydrophobic
			— (αE)	Met115	CE	3.96	hydrophobic
		CZ	— (αF)	Ala161	CB	3.78	hydrophobic
(αE)	Glu120	OE2	— (αE)	Tyr111	OH	3.35	H-bond
(αE)	Tyr123	CE2	— (αE)	Tyr111	CD2	3.85	hydrophobic
			— (αF)	Val158	CG2	3.89	hydrophobic
		CZ	— (αF)	Val158	CG2	3.74	hydrophobic
		OH	—	Ala103	O	2.56	H-bond
	Ser148	O	— (αF)	Gln168	NE2	3.01	H-bond
	Ala150	O	— (αF)	Arg171	NH1	3.43	H-bond
	Leu151	O	— (αF)	Gln168	NE2	3.03	H-bond
	Ala152	CB	— (αF)	Phe175	CD2	3.93	hydrophobic
(αF)	Ala161	CB	— (αE)	Phe119	CZ	3.89	hydrophobic
			— (αF)	Ala165	CB	4.09	hydrophobic
(αF)	Ala165	CB	— (αF)	Ala161	CB	4.10	hydrophobic
			— (αF)	Ala165	CB	4.07	hydrophobic
(αF)	Gln168	NE2	—	Ser148	O	3.09	H-bond
			—	Leu151	O	3.12	H-bond
(αF)	Leu173	CD2	—	Ala103	CB	3.72	hydrophobic
(αF)	Phe175	CD2	—	Ala152	CB	3.94	hydrophobic
(αF)	Glu176	OE2	—	Ala103	N	2.90	H-bond

of αG" may be fixed in the complex. In addition, Glu205, which is the N-terminal residue of αG' and interacted with an adjacent subunit in the unliganded crystal, makes a hydrogen bond with Tyr156 located in the core domain of the same subunit in this structure. This interaction may act as a lock for the proper positioning of αG" in the complex. These results suggest that αG", which locates near the TR-II active site, swings while the substrate and the cofactor do not bind at the active site, and when the cofactor binds, αG" is fixed and complete the active site. This fixed αG" is also considered to provide the coplementarity for the substrate binding, which is important for the substrate recognition (described below).

The 2'-phosphate group of the adenine ribose in $NADP^+$ make electrostatic and hydrogen-bonding interactions with Arg19 and Arg41. These residues changed their side chain conformations from the unliganded TR-II. Especially, in the ternary complex, the side chain of Arg19 flips toward the 2'-phosphate group from the position in the unliganded structure, which interacts with Thr194. In the complex structure, the Cα position of Thr194 moved 1.18 Å from the position in the unliganded structure, in which αG" does not position properly for catalysis. Therefore removing the interaction of Arg19 with Thr194 also seems to be responsible for proper αG" positioning. Arg41 is located at the N-terminal side loop of αC. Since αC (residues 43-55) is one of the segment which changes the position largely from the unliganded structure (Figure 4-6), the conformational change of the side chain of Arg41 may be responsible for the movement of αC.

Other interactions with $NADP^+$ present in this structure are similar to those in the TR-I structure complexed with $NADP^+$ (Nakajima *et al.*, 1998), or other structures of SDR enzymes complexed with a cofactor or with both a cofactor and a substrate (Varughese *et al.*, 1992; Su *et al.*, 1993; Ghosh *et al.*, 1994; Rafferty *et al.*, 1995; Andersson *et al.*, 1996; Breton *et al.*, 1996; Tanaka *et al.*, 1996a; Tanaka *et al.*, 1996b).

Ψ-Tropine Binding Site

To be exact, this TR-II ternary complex was in a certain equilibrium state between before (complexed with $NADP^+$ and ψ-tropine) and after (complexed with NADPH and tropinone) the reverse reaction. To determine the equilibrium state, TR-II in solution was allowed to react to reach the equilibrium in two different conditions: one which is similar to the crystallization condition (the reverse reaction condition), and another which is similar but containing NADPH and tropinone instead of $NADP^+$ and ψ-tropine (the forward reaction condition). Then NADPH contents in the solutions were measured. Both solutions of the reverse and forward reaction condition reached an equilibrium about 4 days after the reaction beginning, and they exhibited a

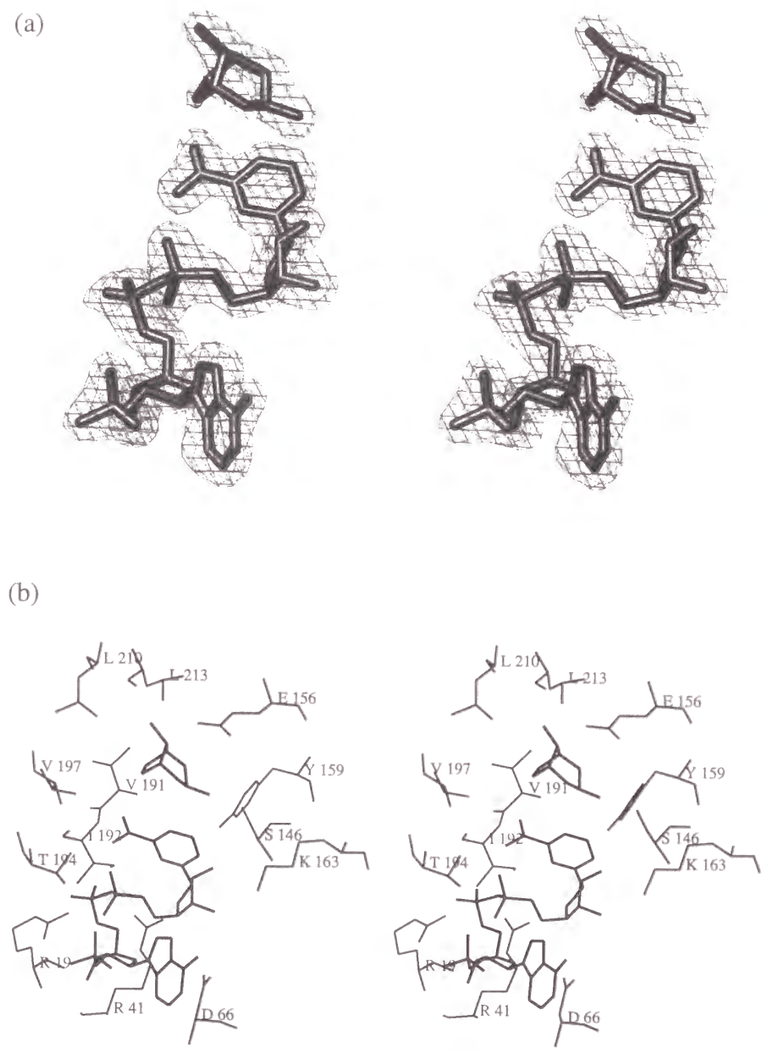

Figure 4-7. (a) Stereoview of the electron density map at 1.9 Å resolution for the ligands, $NADP^+$ and ψ-tropine at the active site in subunit A. The F_O -F_C omit map, contoured at the 3.5 σ level, was calculated with the refined model excluding the ligands. (b) Stereoview of the ψ-tropine and $NADP^+$ binding sites. ψ-Tropine (above) and $NADP^+$ (below) is illustrated in thick lines. The figures were produced with TURBO-FRODO (Bio-Graphics).

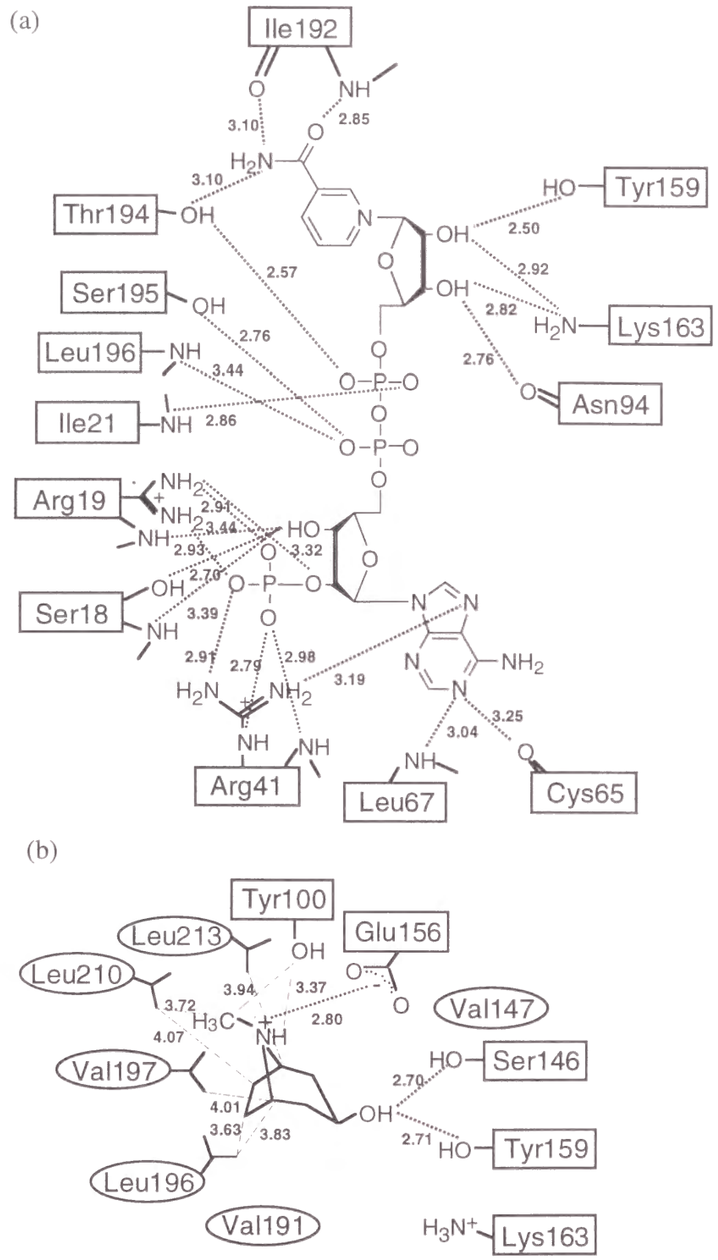

Figure 4-8. (a) Schematic view of the interactions of $NADP^+$ with TR-II. Hydrogen bonds are indicated with dashed lines. The distances (observed in subunit A, ≤ 3.4 Å) are in angstroms. (b) Schematic view of the interactions of ψ-tropine with TR-II. Hydrogen bonds are indicated with dashed lines. Up to 4.1 Å for van der Waals contacts, indicated with thin dot and dashed lines, were used (Sheriff *et.al.*, 1987). The distances (observed in subunit A) are in angstroms.

similar proportion between $NADP^+$ and NADPH; the proportions of NADPH to total dinucleotide contents in the both reverse and forward reaction conditions were 4.1 % after 10 days incubation. The results suggest that more than 95 % TR-II molecule in the crystal existed as a complex with $NADP^+$ and ψ-tropine. Thus ψ-tropine models rather than a tropinone models were used in the refinement process and further discussion.

The ψ-tropine molecule was found in the cleft between the small lobe and the core structure and above the B face of nicotinamide ring of the $NADP^+$ molecule. The electron density map showed the piperidine ring to be in the chair form with the CH_3 group on the nitrogen atom in equatorial position with respect to this ring. The conformation of ψ-tropine in the binding site was the same as its crystallographic structure (Schenk *et al.*, 1967). The binding site is surrounded by the hydrophobic residues, Val147, Val191, Leu196, Val197, Leu210, Leu213, most of which are located in helices αG'' (195-201) and αG' (204-210) (Figure 4-8b). Since these residues are positioned near the non-polar part of ψ-tropine such as the methyl group and the C6-C7 methylene bridge, a significant part of the binding energy is likely to be derived from these hydrophobic interactions. Some residues are in van der Waals contacts with the ψ-tropine molecule (Figure 4-8b). Nearly 98 % of the 299 $Å^2$ accessible surface area of the ψ-tropine is buried in the binding site.

Enzymes of the SDR family contain a highly conserved Ser-Tyr-Lys triad at the active site and the mechanistic proposals have focused on the central role of these residues in catalysis (Ghosh *et al.*, 1994; Ghosh *et al.*, 1995; Rafferty *et al.*, 1995; Andersson *et al.*, 1996; Azzi *et al.*, 1996; Breton *et al.*, 1996; Tanaka *et al.*, 1996a; Tanaka *et al.*, 1996b). These conserved residues are in fact located around the hydroxyl group of ψ-tropine in the ternary complex of TR-II (Figure 4-7b, 4-8b). The distance between the hydroxyl group of ψ-tropine and Tyr159 Oη suggests that Tyr159 should be able to act as a general acid/base catalyst in the TR-II active site. Ser146 is considered to make hydrogen bonding with the hydroxyl group of ψ-tropine from the opposite direction of Tyr159. The distance between Lys163 Nη and Try159 Oη is 4.32 Å, and Lys163 could reduce the p*Ka* of Tyr159 by electrostatic interaction. In addition, Lys163 is also responsible for $NADP^+$ binding (Figure 4-8a). These findings are almost in agreement with the mechanism proposed in other SDR enzymes.

The ψ-tropine binding mode observed in this structure is also in accordance with the proposed mechanism for the differentiation of the stereospecificity of TRs which was assumed from their unliganded structures in CHAPTER 3. In this ternary complex, ψ-tropine binds to the enzyme orienting its α side toward the B-face of the $NADP^+$ (Figure 4-7b). In this binding position, Glu156 is located near the amine moiety of ψ-tropine. The electrostatic interaction

between the positive charge of the amine moiety of the substrates and the negative charge of Glu156 is likely to fix the binding orientation of the substrates properly for producing β-hydroxyl group in tropinone reduction of TR-II.

Furthermore, the binding site shows the complementarity for the substrate binding in correct orientation. Figure 4-9 shows the active sites of TR-II and TR-I. Tropinone bound in TR-II active site is modeled using the tropane ring of bound ψ-tropine in the TR-II ternary complex. Tropinone bound in the TR-I active site is predicted as follows: the tropinone molecule is turned over and superimposed its carbonyl plane with the original one so as to maintain the geometry of the carbonyl plane toward the *pro-S* hydride of NADPH and the catalytic tyrosine residue. As shown in Figure 4-9, TR-II and TR-I have different shapes of voids for substrate binding, and this difference comes from different kinds of residues at the similar position such as Val153 (TR-II) and Leu165 (TR-I), Leu210 (TR-II) and Ile223 (TR-I), and Leu213 (TR-II) and Phe226 (TR-I). These voids fits the tropinone molecules binding in the correct orientations for the respective enzymes (Figure 4-9). Especially, the binding sites have complementary pockets for the C6-C7 methylene bridge of tropinone at the corresponding positions. If tropinone binds to TR-II in opposite orientation, steric clashes between the methylene bridge and Glu156 would occur. On the other hand, if tropinone binds to TR-I in opposite orientation, it does not fit well to the binding site and small openings around tropinone remain in the binding site. These results indicate that the shape of the binding sites together with the electrostatic interactions described above is important for substrate recognition. TR-I has only has charge repulsion, therefore TR-I has longer αG" and compensate for this disadvantage by the rigidity for making the shape of the binding site. In other words, TR-II has strong electrostatic interaction (charge attraction), therefore it adopts more flexible structure and facilitates the turnover.

Active Site Architecture and Implication for Catalysis

The structure of TR-II ternary complex also sheds light on the catalytic mechanism for the oxidation of ψ-tropine to tropinone, as the spatial organization of all participants is now completely defined. The reaction implies that the proton transfer to Tyr159 Oη from the hydroxyl group of ψ-tropine, and the nucleophilic attack of the hydride at C3 to the carbon at 4-position of the nicotinamide ring of $NADP^+$ (Figure 4-10a). Since hydrogen positions cannot be seen in electron density maps, the author built the models of the hydrogen atoms on O3 and on C3, defined as H_O and H_C, respectively, using QUANTA (Molecular Simulations Inc.) with the theoretical O-H and C-H bond lengths. The position of H_C atom could be determined

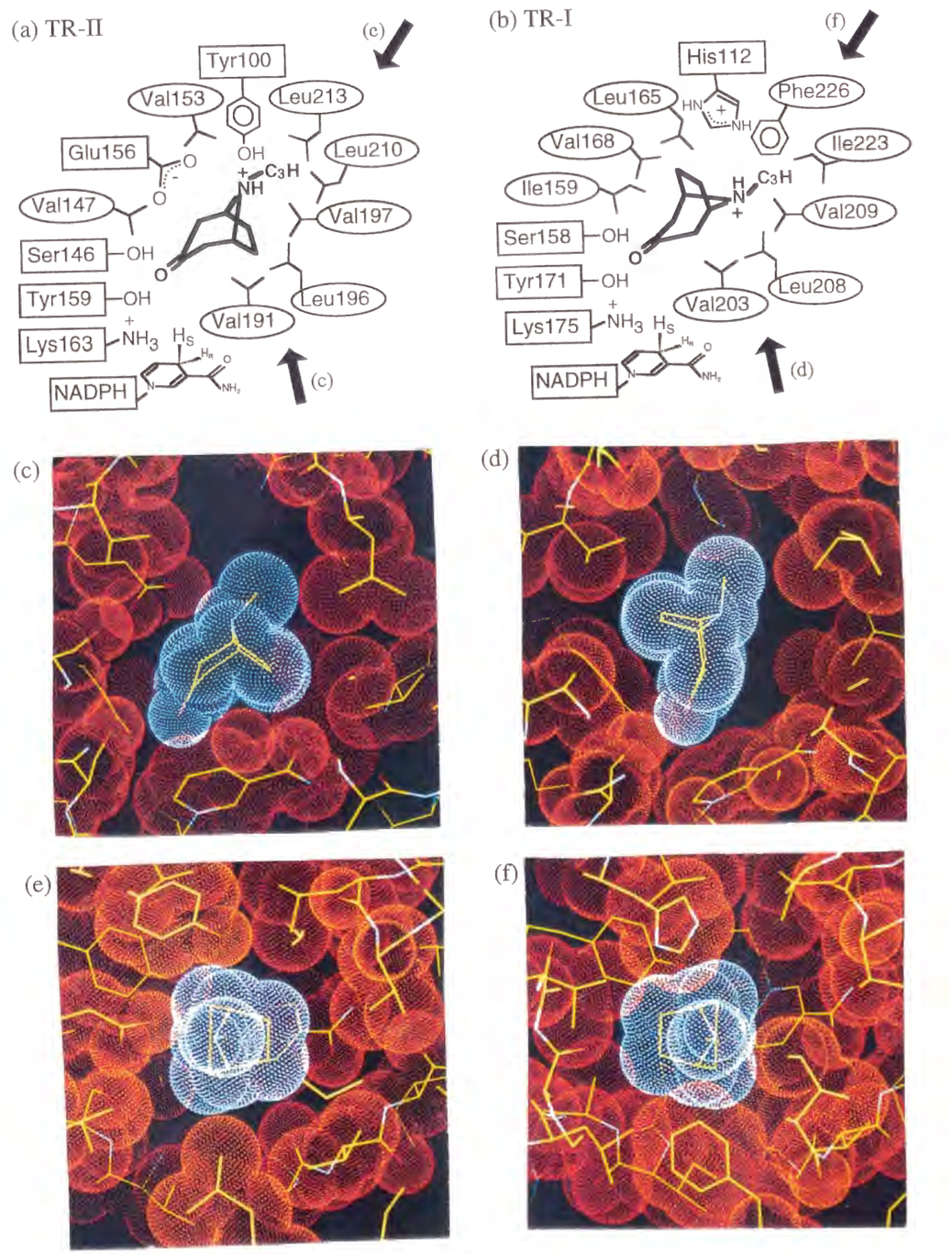

Figure 4-9. (a), (b) Schematic view of the active sites. Tropinone is illustrated in thick lines. Black arrows indicates the view directions of Figure 4-9c, d, e and f, respectively. (a) In TR-II. (b) In TR-I. (c), (d), (e), (f) Dotted van der Waals surfaces of the active site cavities. Surfaces of the active sites are shown in red, and surfaces of tropinone are shown in blue. (c), (e) In TR-II. (d), (f) In TR-I. Figures are generated with TURBO-FRODO.

unequivocally with the theoretical tetrahedral coordinate of carbon atom. Though the C3-O3 bond can rotate freely, the H_O atom was assumed to be at the closest position to Tyr159 Oη, since the proton transfer is likely to occur when the H_O takes the closest position to Tyr159 Oη. Thus, the H_O position was expected to be 1.75 Å apart from Tyr159 Oη in subunit A.

The dihedral angle between C4-C3-O3-H_O is observed as 47.3 °. In this geometry, the lone pair of O3 is likely to be almost *anti*-periplanar to H_C. This result suggests that the position of Tyr159 makes the orbitals on O3 align properly by interacting with H_O and provides favorable condition for H_C eliminating (Figure 4-10b). The side chain of Tyr159 changed its conformation slightly from the unliganded structure (the difference of the χ_1 angle is - 6.0 °) , and seems to take this favorable position because of the interactions with ψ-tropine O3 and $NADP^+$ O2'N when the substrates bind. Besides, the angle between N-C4-H_C is observed as 101.4 ° (Figure 4-10b). The hydride attack angles in the model transfer reactions and in dehydrogenase reactions have been calculated with various computational methods, and in most cases this angle was calculated as obtuse angles between 102 ° and 119 ° (Wu and Houk, 1987a; Wu and Houk, 1987b; Wu and Houk, 1987c; Sherrod and Menger, 1989). Wu and Houk explained that these angles were determined by the effects of maximizing the overlap of a hydride HOMO with the LUMO of one electrophilic C=X species and of minimizing interaction

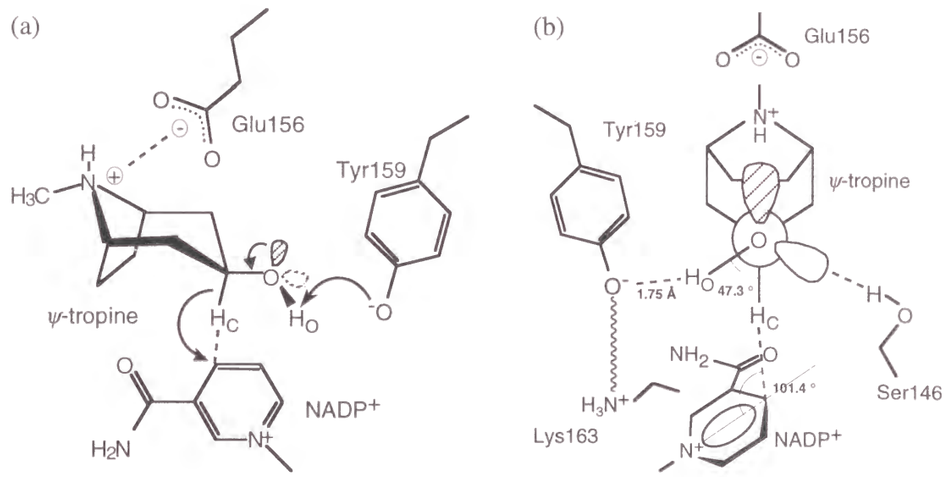

Figure 4-10. Schematic representation for the proposed mechanism of the oxidation reaction of ψ-tropine to tropinone. (a) The reaction implies the transfer of the ψ-tropine O3 proton (H_O) to Tyr159 Oη, and the nucleophilic attack of the ψ-tropine C3 hydride (H_C) on the nicotinamide C4 of $NADP^+$. (b) Orthogonal view of (a) along O3-C3 bond of ψ-tropine. The spatial organization of TR-II catalytic residues, $NADP^+$, ψ-tropine and its orbitals are illustrated.

of the hydride HOMO with the C=X HOMO (Wu and Houk, 1987c). Thus the N-C4-H_C angle seen in the TR-II ternary complex is considered to be appropriate for the hydride attack on the $NADP^+$ nicotinamide ring. These results suggest that the active site architecture places the orbitals which are responsible for the reaction in the most favored positions for the reaction proceeding in terms of stereoelectronic effects.

In practice, however, the ψ-tropine oxidation reaction is in the reverse direction of the metabolic pathway, and its reaction rate is much slower than the tropinone reduction rate in TR-II (Hashimoto *et al.*, 1992). This property is only seen in TR-II, since TR-I or other SDR enzymes can catalyze both oxidation and reduction reaction with comparable rates. One of the possibilities which cause this phenomenon seems to be the existence of Glu156 at the active site; negative charge of Glu156 may destabilize the deprotonated state of Tyr159 which is needed prior to the reverse reaction. In addition Glu156 may make hydrogen bond with the H_O atom of ψ-tropine, and may disturb the orbital alignment which is favored for the reaction as described above. In TR-I, a residue corresponding to the Glu156 is Val168 and the non-polar valine residue cannot interact with Tyr171 or the hydroxyl group of the substrate.

The structure of TR-II complexed with $NADP^+$ and ψ-tropine revealed the active site architecture of this enzyme and the structure of the bound substrates. The part of the active site in TR-II, αG", is flexible in the unliganded enzyme, however, is observed as ordered structure in the ternary complex. Therefore, the active site seems to be completed properly for the catalytic reaction when the substrates bind. The active site architecture in the ternary complex also indicated that it provides the spatial organization to maintain its stereospecificity and to make the catalytic reaction favorable.

CHAPTER 5

General Conclusion

In this study, structural basis for the reaction mechanism of TR-II has been analyzed using X-ray crystallographic techniques. Two crystal structures of TR-II have been determined in this study; the unliganded TR-II and the ternary complex of TR-II with $NADP^+$ and ψ-tropine. Consequently, it has been elucidated not only the catalytic functions but also the factors for maintaining the stereospecificity based on these structures.

First the TR-II structure was determined using the MIR method in order to elucidate its overall structure (CHAPTER 2 and CHAPTER 3). The TR-II crystals were obtained using MPD and ammonium phosphate as precipitants with the hanging-drop vapor diffusion method. The cryocrystallographic technique made it possible to collect a complete diffraction dataset from these crystals. The crystals belong to the space group of $P4_22_12$ with the cell dimensions of $a = b = 62.8$ Å and $c = 128.4$ Å. Phase determination was carried out using the $KAu(CN)_2$- and the $HgCl_2$-derivative crystals. The structure model was refined to the R-factor of 20.5 % with the reflections between 10.0 and 2.3 Å resolution. The structure showed that TR-II is an α/β doubly wound protein with the Rossmann-fold for NADPH binding.

The TR-II ternary complex structure with $NADP^+$ and ψ-tropine was further determined in order to explicate the active site structure and the substrates binding mode (CHAPTER 4). The complex crystals were obtained using lithium sulfate as the precipitant with the hanging-drop vapor diffusion method. The crystals belong to the space group of $P6_122$ with the cell dimensions of $a = b = 88.59$ Å and $c = 338.34$ Å. Structure determination was carried out using the MR method, and the structure model of the complex was refined to the R-factor of 17.2 % with the reflections between 10.0 and 1.9 Å resolution. The complex structure identified the cofactor and the substrate binding site in TR-II, binding mode of the cofactor and the substrate, and the residues responsible for catalytic functions.

These two TR-II structures together with the TR-I structure, which was analyzed by our collaborators, has given insights into the reaction stereospecificity of these enzymes. TR-II and TR-I have strikingly similar overall structures and the NADP(H) binding sites. The $NADP^+$ binding mode observed in the complex structures is also common to both TRs; the nicotinamide rings are in the *syn* conformation. These findings are consistent with the results reported so far that two TRs show similar affinities and the same stereospecificities (*pro-S* hydride transfer) for

NADPH (Hashimoto *et al.*, 1992). In addition, the catalytic residues, such as Tyr159, Ser146 and Lys163 in TR-II, are conserved at similar positions in both enzymes. On the basis of these result, TR-II and TR-I are considered to bind the substrate at same position but directing opposite faces toward NADPH in order to differentiate their reaction stereospecificities. The substrate binding mode observed in the TR-II ternary complex structure was in good agreement with this stereospecific reaction mechanism; the α face of the substrate was directed towards the nicotinamide ring for hydride transfer involving a β-oriented hydroxyl group.

For differentiation of the substrate binding modes, TR-II and TR-I provide different architectures for the substrate binding sites. The substrate orientation in TRs seems to be controlled by two ways: one is molecular recognition by van del Waals contacts with hydrophobic residues, and the other is electrostatic interactions between the substrate and polar residues. The substrate binding sites in TR-II and TR-I have different shapes of voids, which are made by different kinds of hydrophobic residues. These sites furnish the complementarity for the substrates binding in correct orientations. These substrate orientations are further supported by polar interactions at the binding sites. In TR-II, Glu156 is likely to interact electrostatically with the amine moiety of the substrate and fix the binding orientation described above. On the other hand, in TR-I, Glu156 is replaced by Val168 and there is His112 instead of Tyr100 in TR-II. Therefore, in TR-I, the substrate is considered to bind in the opposite orientation of that in TR-II, in order to avoid charge repulsion between His112 and the amine moiety of the substrate. To summarize, the two TRs conserve their protein frameworks to maintain the same reaction mechanism, but provide different environments for the substrate binding by changing several residues in order to differentiate the reaction stereospecificity.

The structure of the TR-II ternary complex further elucidated detailed aspects of the catalytic mechanism of TR-II. The spatial organization of the substrate, the cofactor and the catalytic residues indicated that the active site places the molecular orbitals which are responsible for the reaction, such as the orbitals on O3 and C3, in the most favored positions for the reaction to proceed. This alignment is in line with the concept of stereoelectronic effect. In addition, the presence of the segment (αG"), which is disordered in the unliganded enzyme but constitutes the active site in the complex, suggested that TR-II adopts a flexible structure to facilitate the substrate turnover and serves proper architecture for the catalytic reaction when the substrate bind at the active site.

Acknowledgements

The present thesis is based on the studies carried out from 1995 to 1998 at Institute for Chemical Research, Kyoto University.

The author wishes to express her sincere and heartfelt gratitude to Professor Jun'ichi Oda, Institute for Chemical Research, Kyoto University, for his continuous guidance and encouragement throughout this study.

The author is deeply indebted to Dr. Hiroaki Kato, Instructor of Institute for Chemical Research, Kyoto University, for his invaluable advice and discussions throughout this investigation and also for his critical reading of the manuscript. The author expresses her heartful gratitude to Dr. Toru Nakatsu, Associate Instructor of Institute for Chemical Research, Kyoto University, for his constant advice and precious discussions. The author also wishes to thank to Associate Professor Jun Hiratake, Institute for Chemical Research, Kyoto University, for his helpful suggestion and advice.

The author is very much grateful to Professor Yasuyuki Yamada, Nara Institute of Science and Technology, for his continuous guidance in this study. The author is much indebted to Dr. Keiji Nakajima, Research Associate of Nara Institute of Science and Technology, for his invaluable advice and discussions. The author wishes to thank Associate Professor Takashi Hashimoto and Mr. Hiroyuki Akama, Nara Institute of Science and Technology, for their collaboration in this study. The author also thanks to Professor Takaaki Nishioka, Faculty of Agriculture, Kyoto University, for introducing the author to this study.

The author wishes to express her grateful acknowledgement to Dr. Soichi Wakatsuki and Mr. Takashi Tomizaki, European Synchrotron Radiation Facility, for data collection from the complex crystals, data reduction, and precious discussions. The author is also much indebted to Dr. Wakatsuki for his critical reading of the manuscript.

The author gratefully thanks to Associate Professor Yasuo Hata and Dr. Tomomi Fujii, Instructor, Institute for Chemical Research, Kyoto University, for their helpful suggestions and supporting instrumentation. The author also wishes to thank Associate Professor Bunzo Mikami, Institute for Food Science, Kyoto University, for his advice in amino acid analysis and invaluable suggestions in X-ray crystallography. Computational support by Super Computer Laboratory, Institute for Chemical Research, Kyoto University, is also acknowledged.

The author wishes to thank Dr. Yuichiro Maéda and Dr. Katsumi Imada, International Institute for Advanced Research, Matsushita Electric Industrial Co., Ltd., for their advice in

cryocrystallographic experiments. The author also wishes to thank Dr. Naoki Kunishima and Dr. Koske Morikawa, Biomolecular Engineering Research Institute, for their advice in structure refinement. The author also thanks to Associate Professor Atsushi Nakagawa, Hokkaido University, for his helpful discussions and advice.

A special debt of gratitude goes to Professor Hajime Iwamura and Associate Professor Hideto Miyoshi, Faculty of Agriculture, Kyoto University, for their kind encouragement.

The author thanks to Dr. Hiroyuki Shibata for his advice in enzyme purification experiments, and to Mr. Masaaki Sawa for his advice in ψ-tropine synthesis. The author also thanks to all the members of Laboratory of Molecular Conversion Chemistry, Division of Biofunctional Molecules, Institute for Chemical Research, Kyoto University, for their kind supports and encouragement throughout this study.

Finally, the author is very grateful to her friends and brothers for their warm encouragement, and to her parents, Katsuhiro Yamashita and Toshiko Yamashita, for incessant encouragement and support.

References

Andersson, A., Jordan, D., Schneider, G. and Lindqvist, Y. (1996) *Structure*, **4**, 1161-1170.

Azzi, A., Rehse, P. H., Zhu, D. W., Campbell, R. L., Labrie, F. and Lin, S. X. (1996) *Nature Struct. Biol.*, **3**, 665-668.

Bauer, A. J., Rayment, I., Frey, P. A. and Holden, H. M. (1992) *Proteins*, **12**, 372-381.

Bijvoet, J. M. (1954) *Nature*, **173**, 888-891.

Boyer, P. D. (ed.) (1975) *The Enzymes*, Academic Press, New York, Vol. XI.

Bradford, M. M. (1976) *Anal. Biochem.*, **72**, 248-254.

Breton, R., Housset, D., Mazza, C. and Fontecilla-Camps, J. C. (1996) *Structure*, **4**, 905-915.

Bricogne, G. (1976) *Acta Cryst.*, **A32**, 832-847.

Bricogne, G. (1991) *Acta Cryst.*, **A47**, 803-829.

Brünger, A. T. (1992a) *Nature*, **355**, 472-475.

Brünger, A. T. (1992b) *X-PLOR Manual Version 3.1.* Yale University Press, New Havenm CT.

Brünger, A. T., Krukowski, A. and Erickson, J. (1990) *Acta Cryst.*, **A46**, 585-593.

Brünger, A. T., Kuriyan, J. and Karplus, M. (1987) *Science*, **235**, 458-460.

Chen, Z., Jiang, J. C., Lin, Z. G., Lee, W. R., Baker, M. E. and Chang, S. H. (1993) *Biochemistry*, **32**, 3342-3346.

Collaborative Computational Project, No.4 (1994) *Acta Cryst.*, **D50**, 760-763.

Cols, N., Marfany, G., Atrian, S. and Gonzàlez-Duarte, R. (1993) *FEBS Lett.*, **319**, 90-94.

Cudney, B., Patel, S., Weisgraber, K., Newhouse, Y. and McPherson, A. (1994) *Acta Cryst.*, **D50**, 414-423.

Drenth, J. (1994) In *Principles of Protein X-ray Crystallography*, Springer-Verlag, New York, pp. 129-182.

Engh, R. A. and Huber, R. (1991) *Acta Cryst.*, **A47**, 392-400.

Ensor, C. M. and Tai, H. H. (1991) *Biochem. Biophys. Res. Commun.*, **176**, 840-845.

Furey, W. and Swaminathan, S. (1997) In Carter, C. and Sweet, R. (eds.), *Methods Enzymol.*, **277**, 590-620.

Ghosh, D., Pletnev, V. Z., Zhu, D. W., Wawrzak, Z., Duax, W. L., Pangborn, W., Labrie, F. and Lin, S. H. (1995) *Structure*, **3**, 503-513.

Ghosh, D., Wawrzak, Z., Weeks, C. M., Duax, W. L. and Erman, M. (1994) *Structure*, **2**,

629-640.

Goldberg, J. D., Yoshida, T. and Brick, P. (1994) *J. Mol. Biol.*, **236**, 1123-1140.

Green, D. W., Ingram, V. M. and Perutz, M. F. (1954) *Proc. R. Soc. London*, **A225**, 287-307.

Hanahan, D. (1983) *J. Mol. Biol.*, **166**, 557-580.

Hashimoto, T., Nakajima, K., Ongena, G. and Yamada, Y. (1992) *Plant Physiol.*, **100**, 836-845.

Higgins, D. G., Bleasby, A. J. And Fuchs, R. (1992) *CABIOS*, **8**, 189-191.

Hope, H. (1988) *Acta Cryst.*, **B44**, 22-26.

Hope, H. (1990) *Annu. Rev. Biophys. Biophys. Chem.*, **19**, 107-126.

Jancarik, J. and Kim, S. H. (1991) *J. Appl. Cryst*, **24**, 409-411.

Jörnvall, H., Persson, B., Krook, M., Atrian, S., Gonzàlez-Duarte, R., Jeffert, J. and Ghosh, D. (1995) *Biochemistry*, **34**, 6003-6013.

Jörnvall, H., Persson, M. and Jeffery, J. (1981) *Proc. Natl. Acad. Sci. USA*, **78**, 4226-4230.

Kiefer, P. M., Grimshaw, C. E. and Whiteley, J. M. (1997) *Biochemistry*, **36**, 9438-9445.

Kiefer, P. M., Varughese, K. I., Su, Y., Xuong, N. H., Chang, C. F., Gupta, P., Bray, T. and Whiteley, J. M. (1996) *J. Biol. Chem.*, **271**, 3437-3444.

Kraulis, P. J. (1991) *J. Appl. Cryst.*, **24**, 946-950.

Kletwegt, G. J. and Jones, T. A. (1997) *Methods Enzymol.*, **277**, 208-230.

Laemmli, U. K. (1970) *Nature*, **227**, 680-685.

Lamzin, V. S., Dauter, Z., Popov, V. O., Harutyunyan, E. H. and Wilson, K. S. (1994a) *J. Mol. Biol.*, **236**, 759-785.

Lamzin, V. S., Dauter, Z. and Wilson, K. S. (1994b) *Nature Struct. Biol.*, **1**, 281-282.

Lamzin, V. S., Dauter, Z. and Wilson, K. S. (1995) *Curr. Opin. Struct. Biol.*, **5**, 830-836.

Laskowski, R. A., MacArthur, M. W., Moss, D. S. and Thornton, J. M. (1993) *J. Appl. Cryst*, **26**, 283-291.

Liu, Y., Thoden, J. B., Kim, J., Berger, E., Gulick, A. M., Ruzicka, F. J., Holden, H. M. and Frey, P. A. (1997) *Biochemistry*, **36**, 10675-10684.

Luzzati, P. V. (1952) *Acta Cryst.*, **5**, 802-810.

Matthews, B. W. (1968) *J. Mol. Biol.*, **33**, 491-497.

Moffat, K. and Henderson, R. (1995) *Curr. Opin. Struct. Biol.*, **5**, 656-663.

Murshudov, G. N., Vagin, A. A. and Dodson, E. J. (1997) *Acta Cryst.*, **D53**, 240-255.

Nakajima, K., Hashimoto, T. and Yamada, Y. (1993) *Proc. Natl. Acad. Sci. USA*, **90**,

9591-9595.

Nakajima, K., Hashimoto, T. and Yamada, Y. (1994) *J. Biol. Chem.*, **269**, 11695-11698.

Nakajima, K. (1997) thesis, Kyoto University.

Nakajima, K., Yamashita, A., Akama, Y., Nakatsu, T., Kato, H., Hashimoto, T., Oda, J. and Yamada, Y. (1998) *Proc. Natl. Acad. Sci. USA,* in press.

Nakanishi, M., Kakumoto, M., Matsuura, K., Deyashiki, Y., Tanaka, N., Nonaka, T., Mitsui, Y. and Hara, A. (1996) *J. Biochem.*, **120**, 257-263.

Navaza, J. (1994) *Acta Cryst.*, **A50**, 157-163.

Nicholls, P. J., Sharp, K. A. And Honig, B. (1991) *Proteins Struct. Funct. Genet.*, **11**, 281-296.

Nickson, A. and Fieser, L. F. (1952) *J. Am. Chem. Soc.*, **74**, 5566-5570.

Obeid, J. and White, P. C. (1992) *Biochem. Biophys. Res. Commun.*, **188**, 222-227.

Otwinowski, Z. (1993) In Sawyer, L., Isaacs, N. and Bailey, S. (eds.), *CCP4 Study Weekend: Data Collection and Processing*, SERC Daresbury Laboratory, Warrington, England, pp. 56-62.

Patterson, A. L. (1934) *Phys. Rev.*, **46**, 372.

Petsuko, G. A. (1975) *J. Mol. Biol.*, **96**, 381-392.

Portsteffen, A., Dräger, B. and Nahrstedt, A. (1994) *Phytochemistry*, **37**, 391-400.

Rafferty, J. B., Simon, J. W., Baldock, C., Artymiuk, P. J., Baker, P. J., Stuitje, A. R., Slabas, A. R. and Rice, D. W. (1995) *Structure*, **3**, 927-938.

Read, R. J. (1986) *Acta Cryst.*, **A42**, 140-149.

Read, R. J. (1990) *Acta Cryst.*, **A46**, 900-912.

Rodgers, D. W. (1994) *Structure*, **2**, 1135-1140.

Rodgers, D. W. (1997) *Methods Enzymol.*, **276**, 183-203.

Rossmann, M. G., Adams, M. J., Buehner, M., Ford, G. C., Hackert, M. L., Liljas, A., Rao, S. T., Banaszak, L. J., Hill, E., Tsernoglou, D. and Webb, L. (1973) *J. Mol. Biol.*, **76**, 533-537.

Rossmann, M. G. and Blow, D. M. (1962) *Acta Cryst.*, **15**, 24-31.

Rossmann, M. G., Liljas, A., Brändén, C. I. and Banaszak, L. J. (1975) In Boyer, P. D. (ed.) *The Enzymes*, 3rd, Academic Press, New York, Vol. XI, pp. 61-102.

Sato, M., Yamamoto, M., Imada, K., Katsube, Y., Tanaka, N. and Higashi, T. (1992) *J. Appl. Cryst*, **25**, 348-357.

Schenk, S., MacGillavry, C. H., Skolnik, S. and Laan, J. (1967) *Acta Cryst.*, **23**, 423.

Sheriff, S., Hendrickson, W. A. and Smith, J. L. (1987) *J. Mol. Biol.*, **197**, 273-296.

Sherrod, M. J. and Menger, F. M. (1989) *J. Am. Chem. Soc.*, **111**, 2611-2613.

Stoll, V. S., S., K. M. and Pai, E. F. (1996) *Structure*, **4**, 437-447.

Stryer, L., Kendrew, J. C. and Watson, H. C. (1964) *J. Mol. Biol.*, **8**, 96.

Stura, E. A. and Wilson, I. A. (1990) *Methods: A companion to Methods Enzymology*, **1**, 38-49.

Su, Y., Varughese, K. I., Xuong, N. H., Bray, T. L., Roche, D. J. and Whiteley, J. M. (1993) *J. Biol. Chem.*, **268**, 26836-26841.

Sugio, S., Petsko, G. A., Manning, J. M., Soda, K. and Ringe, D. (1995) *Biochemistry*, **34**, 9661-9669.

Tanaka, N., Nanaka, T., Nakanishi, M., Deyashiki, Y., Hara, A. and Mitsui, Y. (1996a) *Structure*, **4**, 33-45.

Tanaka, N., Nonaka, T., Tanabe, T., Yoshimoto, T., Tsuru, D. and Mitsui, Y. (1996b) *Biochemistry*, **35**, 7715-7730.

Teng, T. Y. (1990) *J. Appl. Cryst*, **23**, 387-391.

Thaller, C., Eichele, G., Weaver, L. H., Wilson, E., Karlsson, R. and Jansonius, J. N. (1985) *Methods Enzymol.*, **114**, 132-135.

Varughese, K. I., Skinner, M. W., Whiteley, J. M., Matthews, D. A. and Xuong, N. H. (1992) *Proc. Natl. Acad. Sci. USA*, **89**, 6080-6084.

Vendekerckhove, J., Bauw, G., Puype, M., Damme, V. J. and Montagu, M. (1985) *Eur. J. Biochem.*, **152**, 9-19.

Wang, B. C. (1985) *Methods Enzymol.*, **115**, 90-112.

Watenpaugh, K. D. (1991) *Curr. Opin. Struct. Biol.*, **1**, 1012-1015.

Wu, Y. D. and Houk, K. N. (1987a) *J. Am. Chem. Soc.*, **109**, 906-908.

Wu, Y. D. and Houk, K. N. (1987b) *J. Am. Chem. Soc.*, **109**, 908-910.

Wu, Y. D. and Houk, K. N. (1987c) *J. Am. Chem. Soc.*, **109**, 2226-2227.

List of Publications

Chapter 2

Atsuko Yamashita, Keiji Nakajima, Hiroaki Kato, Takashi Hashimoto, Yasuyuki Yamada and Jun'ichi Oda

"Crystallization and preliminary crystallographic study of tropinone reductase-II from *Datura stramonium*", submitted.

Chapter 3

Keiji Nakajima, Atsuko Yamashita, Hiroyuki Akama, Toru Nakatsu, Hiroaki Kato, Takashi Hashimoto, Jun'ichi Oda and Yasuyuki Yamada

"Crystal structures of two tropinone reductases: different reaction stereospecificities in the same protein fold", (1998) *Proc. Natl. Acad. Sci. USA*, **95**, in press.

Chapter 4

Atsuko Yamashita, Hiroaki Kato, Soichi Wakatsuki, Takashi Tomizaki, Toru Nakatsu, Keiji Nakajima, Takashi Hashimoto, Yasuyuki Yamada and Jun'ichi Oda.

"Structure of tropinone reductase-II complexed with $NADP^+$ and pseudotropine at 1.9 Å resolution: Implication for catalysis", manuscript in preparation.